J. Fluid Mech. (2022), *vol*. 949, A28, doi:10.1017/jfm.2022.752

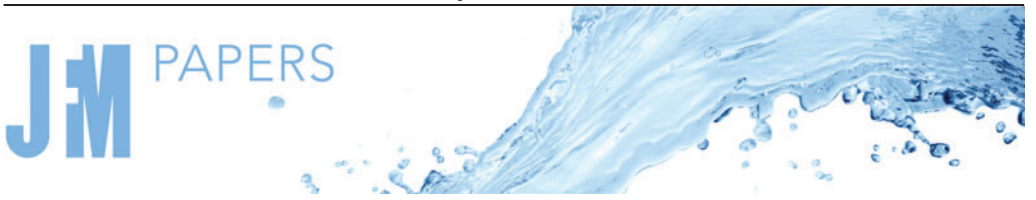

The role of vibrations for reducing the resistance in the relative movement of parallel plates

J.M. Floryan[1],† **and N.N. Haq**[1]

[1]Department of Mechanical and Materials Engineering, The University of Western Ontario, London, Ontario N6A 5B9, Canada

(Received 1 March 2022; revised 19 August 2022; accepted 29 August 2022)

The effect of surface vibrations on the propulsion augmentation and resistance in the relative movement of parallel plates has been studied. The analysis was focused on monochromatic waves and laminar flows. The effectiveness of the vibrations was gauged by determining the external force required to maintain the movement of one of the plates at a prescribed velocity. It is shown that waves propagating upstream always increase the resistance but the flow response to waves propagating downstream is more intricate and is a function of the flow Reynolds number. In general, waves must be sufficiently fast to reduce the flow resistance. This leads to a natural division between slow and fast waves; a characterization that is helpful for flows at a sufficiently small Reynolds number *Re*. An increase in *Re* brings into play the complication of possible resonances with the natural flow frequencies. Resonances are not possible with waves faster than the plate velocity and these supercritical waves generally decrease the flow resistance. More complex flow responses can occur with slower (subcritical) waves which tend to increase the flow resistance. A complete elimination of the resistance is possible if the waves are of sufficiently short wavelength and travel quickly. This suggests that our mechanism has great potential in the development of propulsion augmentation systems. None of the waves produced net energy savings.

Key words: drag reduction

1. Introduction

The relative movement of two parallel plates is a paradigm for testing new propulsion concepts including the development of strategies for reducing flow resistance or intensifying mixing. This class of flows is of importance in many applications involving the relative motion of components. In these cases, resistance can often be reduced by inserting lubricating fluid between moving surfaces. This both provides energy savings

† Email address for correspondence: floryan@uwo.ca

and can reduce the wear (Gropper, Wang & Harvey 2016). The flow is characterized by the absence of a streamwise pressure gradient, a linear velocity distribution across the gap in the laminar regime and no linear stability limit (Romanov 1972). Shear-driven instabilities may occur in the annular version of this flow (Gittler 1993; Moradi & Floryan 2016). Possible routes to secondary states and to turbulence have been described by Deguchi & Nagata (2011) and Tillmark & Alfredsson (1992). It is known that bypass transition can be initiated by wall transpiration (Floryan 2003), by adding transverse ribs (Floryan 2002) or by using grooves (Mohammadi & Floryan 2014).

An external force needs to be applied to a moving plate in order to maintain its movement, which necessarily implies an expenditure of energy. Our concern in the current work lies with the development of strategies that may lead to a reduction in this loss. In essence, our strategy will aim to generate a propulsion effect that will mean that the magnitude of the required external force can be reduced by way of compensation and will determine if net energy savings are possible. One way this can be achieved is by reducing the shear stresses that act on the moving plate. Our analysis is focused on laminar flows, but the same strategy could be extended to apply to turbulent flows. Various passive approaches have been proposed that may help reduce the resistance to motion. Included in these is the incorporation of surface grooves or corrugations for laminar (Mohammadi & Floryan 2013*a*,*b*, 2014, 2015; Moradi & Floryan 2013; Yadav, Gepner & Szumbarski 2021) and turbulent (Walsh 1983; Chen et al. 2016; DeGroot, Wang & Floryan 2016) flows. An extension of this approach is based on the use of hydrophobic surfaces (Perot & Rothstein 2004). More active techniques involve the application of suitable distributed heating (Hossain, Floryan & Floryan 2012; Floryan & Floryan 2015; Floryan, Shadman & Hossain 2018), wall transpiration (Jiao & Floryan 2021), surface vibrations (Floryan & Zandi 2019), plasma actuators (Inasawa, Ninomiya & Asai 2013), sound (Kato, Fukunishi & Kobayashi 1997) or piezoelectric actuators (Fukunishi & Ebina 2001). An excellent review of some of these ideas has been given by Cattafesta & Sheplak (2011). An obvious question that must be asked when assessing the practicality of the various resistance reduction ideas is whether the energy cost of implementing the method exceeds the likely energy savings resulting from the flow modulations. Laminar unmodulated flow represents the lowest-energy state when modified by wall transpiration (Bewley 2009) but this may not be the case for other control strategies. It is known that modifications of surface topography result in a resistance reduction (Fukagata, Sugiyama & Kasagi 2009; Mohammadi & Floryan 2013*a*,*b*, 2014, 2015; Moradi & Floryan 2013) and can go as far as producing chaotic stirring at energy cost less than that required by unmodified flow (Gepner & Floryan 2020). As our interest is with laminar flow, the reader is reminded that our objective might be achieved indirectly through judicious flow modifications that may prevent the formation of secondary states, thus side-stepping an increase in the flow resistance at larger Reynolds numbers. Such an indirect approach is not followed in this work.

The use of active flow modification can be viewed as an alternative (or distributed) propulsion system in which part of the energy is used to reduce the resistance rather than overcoming it. This device is attractive as it provides a means for improving the performance of a system beyond what might be possible using purely classical propulsion. Any decrease in the wall shear stress, which reduces the long-term wear and thermal stress on bounding surfaces, provides additional benefit. The concept of distributed propulsion is quite familiar in biological systems, e.g. cilia and flagella (Taylor 1951; Blake & Sleigh 1974; Katz 1974; Brennen & Winet 1977; Lauga 2016) and snail locomotion (Chan, Balmforth & Hosoi 2005; Lauga 2007; Lee et al. 2008). These are small-scale objects that move very slowly and so scaling up to practical physical systems is not

necessarily straightforward. The creation of distributed forcing in technical systems involves the imposition of forcing patterns along fluid–solid boundaries to reduce the relative velocity of the two mediums. Known physical manifestations of these effects include nonlinear streaming created by wall transpiration (Jiao & Floryan 2021), the pattern interaction effect (Floryan & Inasawa 2021) that leads to thermal drift (Abtahi & Floryan 2017; Inasawa, Hara & Floryan 2021) and surface vibrations (Floryan & Zandi 2019). Flow relaminarization using transpiration waves (Lieu, Moarref & Jovanović 2010; Moarref & Jovanović 2010; Mamori, Iwamoto & Murata 2014; Kaithakkal, Kametani & Hasegawa 2020) or surface vibrations (Nakanishi, Mamori & Fukagata 2012; Nabae & Fukugata 2021) represent interesting alternatives for the control of turbulent flows.

Vibrations activate the peristaltic effect, the properties of which are of interest to the current analysis. Its basic elements are well known (Fung & Yih 1968; Shapiro, Jaffrin & Weinberg 1969; Jaffrin & Shapiro 1971) and its use to date is based on the Stokes approximation and long-wavelength waves (Lauga 2007, 2016). A recent review of peristaltic flows has been given by Ali, Ullah & Rasool (2020). Until quite recently only waves with phase speeds comparable to those found in various biological systems (such as urine flow from kidney to bladder, movement of food through the digestive tract, transport of ova through fallopian tubes, cilia and flagella, snail movement, etc.) have been explored. The first analysis of short, fast waves has been recently described by Floryan, Faisal & Panday (2021); some earlier work by Hoepffner & Fukagata (2009) considered a few cases of fast waves but their study was restricted to $O(1)$ wavelengths.

The goal of this investigation is to make a systematic analysis of the effects of vibrations on the resistance to the flow between parallel plates in relative motion while avoiding some of the limitations commonly found in the literature such as long-wavelength or small-Reynolds-number approximations. We explore the complete range of wavelengths and phase speeds, but we restrict the size of the vibrations to less than 5 % of the channel opening. This limit is motivated by the fact that our interests are partly with the practical use of piezoelectric actuators which have high-frequency response, but which are characterized by small-amplitude displacements. We also limit the flow Reynolds number to less than 2000 (this quantity is defined in (2.4) below). There is a welter of experimental evidence that Couette flow becomes turbulent at larger Reynolds numbers and our interests are with laminar flows (Tillmark & Alfredsson 1992).

The presence of wall vibrations gives rise to a moving boundary problem with the motion of the boundary prescribed. The sustained character of the vibrations leads to a preference for employing an Eulerian-type algorithm (Floryan & Rasmussen 1989). There are several candidate techniques that might be considered for modelling our time-dependent geometry including the use of numerical grid generation, analytical mappings or boundary condition transfer procedures and the advantages and drawbacks of each of these have been discussed by Cabal, Szumbarski & Floryan (2001). One essential requirement for the present analysis is that both high accuracy and geometric flexibility are required. Given these needs we chose to base our computations on the spectrally accurate immersed boundary conditions (IBC) method (Szumbarski, & Floryan 1999).

The remainder of this paper is structured as follows. First, in § 2, we describe a two-dimensional model problem which takes the form of an infinite slot with a moving smooth upper plate and a lower plate which is subject to a vibration that takes the form of a travelling wave. In § 3 we describe our numerical methods method and illustrate the peristaltic effect.

The scene is set for the remainder of the study in § 4 where we consider the question of resistance reduction. Section 4.1 discusses the global properties of vibration-induced

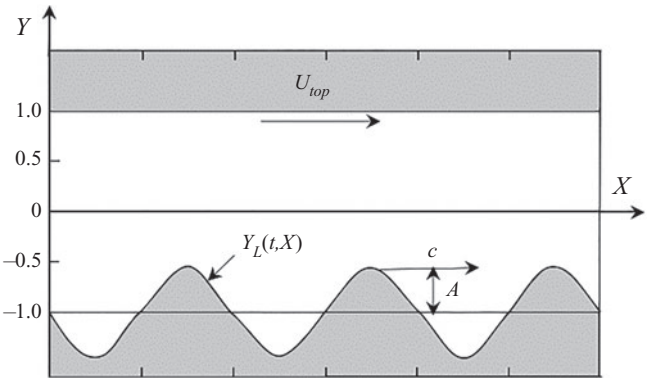

Figure 1. A sketch of the flow configuration.

flow modifications. In §§ 5–7 we consider the behaviours in the cases of slow, medium and fast plate velocities, respectively. The division of the plate velocities in this way is somewhat arbitrary, but we shall see that the properties of the flow do differ between the three classes. Moreover, we also find that as the Reynolds number grows the flow response can be affected by near resonances with the natural flow frequencies. The somewhat complicated picture that emerges is summarized in § 8 which provides a precis of the main conclusions and some associated discussion.

Two rather more technical issues are relegated to appendices in order not to detract from the main flow of the paper. In Appendix A we detail the analytical solution that describes long-wavelength waves. In Appendix B we outline the method used to identify and determine the natural flow frequencies associated with the underlying Couette flow.

2. Problem formulation

To study the effect of vibrations on the resistance present in the relative movement of parallel plates, consider two surfaces that extend to $\pm\infty$ in the X direction and placed a distance $2h$ apart; see figure 1. The lower plate is stationary whilst the upper plate is driven by an external force at a constant prescribed velocity U_{top}. The external force required to maintain this movement provides a measure of the movement resistance. In an attempt to reduce this resistance travelling-wave vibrations are imposed on the lower plate so that the dimensionless slot geometry is defined by

$$Y_U(X,t) = 1, \tag{2.1a}$$

$$Y_L(X,t) = -1 + A\cos[\alpha(X - ct)], \tag{2.1b}$$

where the subscripts U and L refer to the upper and lower plates, respectively, and A is the wave amplitude. Furthermore c and α denote the wave phase speed and wavenumber and the half-mean slot opening h has been adopted as the length scale.

When the system is in a steady state the external force pulling the plate is balanced by the shear force that acts on it. The flow field is determined by solving the Navier–Stokes and continuity equation written the form

$$\frac{\partial u}{\partial t} + u\frac{\partial u}{\partial X} + v\frac{\partial u}{\partial Y} = -\frac{\partial p}{\partial X} + \frac{\partial^2 u}{\partial X^2} + \frac{\partial^2 u}{\partial Y^2},$$
$$\frac{\partial v}{\partial t} + u\frac{\partial v}{\partial X} + v\frac{\partial v}{\partial Y} = -\frac{\partial p}{\partial Y} + \frac{\partial^2 v}{\partial X^2} + \frac{\partial^2 v}{\partial Y^2}, \quad \frac{\partial u}{\partial X} + \frac{\partial v}{\partial Y} = 0, \tag{2.2a–c}$$

where $\boldsymbol{u} = (u, v)$ denotes the velocity vector with components in the (X, Y) directions scaled on $U_v = \nu/h$, where ν denotes the kinematic viscosity. The dimensionless pressure p is scaled on ρU_v^2 and the time t is based on h/U_v; here ρ denotes the fluid density. The relevant boundary conditions are then

$$Y = 1 : \; u = Re, \quad v = 0; \quad Y = Y_L(X, t) : \; u = 0, \quad v = \frac{\partial Y_L}{\partial t}, \tag{2.3a–d}$$

where

$$Re \equiv U_{top} h/\nu \tag{2.4}$$

is the Reynolds number and the normal velocity component at the lower plate is determined by the imposed vibrations. As our interest is in the fluid movement generated by relative movement of the plate as opposed to any pressure gradient that may be present, it is specified that

$$\left.\frac{\partial p}{\partial X}\right|_m = 0, \tag{2.5}$$

where subscript m denotes the mean value. The translation of the upper plate in the absence of any vibrations creates a simple Couette flow. In this motion the dimensionless velocity field $\boldsymbol{v}_0$, pressure p_0, pulling force (per unit length and width) F_0, shear acting on the upper plate τ_0 and the flow rate Q_0 are given by

$$\begin{gathered} \boldsymbol{v}_0(x, y) = [u_0, v_0] = [\tfrac{1}{2}(1 + Y), \; 0], \quad p_0(x, y) = \text{const.}, \quad F_0 = \tfrac{1}{2}, \\ \tau_0 = -\tfrac{1}{2}, \quad Q_0 = 1. \end{gathered} \tag{2.6a–e}$$

Here U_{top} has been adopted as the velocity scale, ρU_{top}^2 as the pressure scale and $U_{top}\mu/h$ as the surface force scale; further the flow rate has also been scaled using U_{top}.

To evaluate the pulling force after the vibrations have been added we integrate the shear stress on the upper plate over a wavelength. The viscous part of the x component of the stress vector $\sigma_{Xv,U}$ that acts on the fluid and the external pulling force (per unit length and width) on the plate F are given by

$$\sigma_{Xv,U} = \left.\frac{\partial u}{\partial Y}\right|_{Y=1}, \quad F = \lambda^{-1} \int_0^{\lambda} \left.\frac{\partial u}{\partial Y}\right|_{Y=1} \mathrm{d}X; \tag{2.7a,b}$$

here the wavelength $\lambda \equiv 2\pi/\alpha$. The ultimate effectiveness of the vibrations depends on their potential to reduce the shear stress at the upper plate – this can be achieved by propelling the fluid through the slot thereby reducing its velocity relative to the moving plate. The propulsion can be generated by a combination of viscous and pressure forces that act on the fluid at the vibrating plate. An appreciation of these forces provides a foundation from which more effective forms of vibrations may be developed. The stress vector at the lower plate $\boldsymbol{\sigma}_L$ is

$$\boldsymbol{\sigma}_L = \begin{bmatrix} \sigma_{X,L} & \sigma_{Y,L} \end{bmatrix} = \begin{bmatrix} n_{X,L} & n_{Y,L} \end{bmatrix} \begin{bmatrix} 2\dfrac{\partial u}{\partial X} - p & \dfrac{\partial u}{\partial Y} + \dfrac{\partial v}{\partial X} \\ \dfrac{\partial u}{\partial Y} + \dfrac{\partial v}{\partial X} & 2\dfrac{\partial v}{\partial Y} - p \end{bmatrix}_{Y=Y_L}, \tag{2.8}$$

where the normal unit vector $\boldsymbol{n}_L$ that points outwards has the form

$$\boldsymbol{n}_L = (n_{X,L}, n_{Y,L}) = N_L \left(\frac{\mathrm{d}Y_L}{\mathrm{d}X}, \; -1 \right), \quad N_L = \left[1 + \left(\frac{\mathrm{d}Y_L}{\mathrm{d}X} \right)^2 \right]^{-1/2}. \tag{2.9a,b}$$

The explicit form of the X component of the stress vector can be written as

$$\sigma_{X,L} = \sigma_{Xv,L} + \sigma_{Xp,L} = N_L \left[2\frac{\mathrm{d}Y_L}{\mathrm{d}X}\frac{\partial u}{\partial X}\bigg|_{Y_L} - \left(\frac{\partial u}{\partial Y} + \frac{\partial v}{\partial X}\right)\bigg|_{Y_L} \right] - N_L \frac{\mathrm{d}Y_L}{\mathrm{d}X} p\bigg|_{Y_L}, \quad (2.10)$$

where $(\sigma_{Xv,L}, \sigma_{Xp,L})$ denote the viscous and pressure contributions, respectively. The X component of the total force $F_{X,L}$ acting on the fluid at the lower plate per unit length is given by

$$F_{X,L} = F_{Xv,L} + F_{Xp,L} = \lambda^{-1} \int_0^\lambda \left[2\frac{\mathrm{d}Y_L}{\mathrm{d}X}\frac{\partial u}{\partial X}\bigg|_{Y_L} - \left(\frac{\partial u}{\partial Y} + \frac{\partial v}{\partial X}\right)\bigg|_{Y_L} \right] \mathrm{d}X$$
$$- \lambda^{-1} \int_0^\lambda \frac{\mathrm{d}Y_L}{\mathrm{d}X} p|_{Y_L}\, \mathrm{d}X, \quad (2.11)$$

where $F_{Xp,L}$ and $F_{Xv,L}$ denote the pressure and viscous contributions.

In what follows it is helpful to monitor the changes in various quantities that result from the inclusion of vibrations rather than tracking the total values themselves. Accordingly, we express the flow field $\boldsymbol{v}$, the pressure p, the mean flow rate Q_{mean}, the shear τ and the pulling force F as

$$\boldsymbol{v}(X, Y) = [u(X, Y), v(X, Y)] = [\tfrac{1}{2}Re(1 + Y) + u_1(X, Y), v_1(X, Y)],$$
$$p(X, Y) = C + p_1(X, Y), \quad (2.12a,b)$$

$$Q_{mean} = Re + Q_{1,mean}, \quad \tau(X) = -\tfrac{1}{2}Re + \tau_1(X), \quad F = \tfrac{1}{2}Re + F_1. \quad (2.12c–e)$$

Then, when there are no vibrations, all the quantities with a subscript 1 are zero. A negative value of F_1 indicates that the resistance is reduced and if we can identify conditions when $F = 0$ this implies that the pulling force is reduced to zero. Of course, a negative value for F would indicate the need to reverse the direction of this force so that the pulling force would need to be replaced by a braking force to maintain the prescribed plate velocity.

3. The solution method

Having developed our model we next set out the numerical strategy that was used to generate the solutions described in subsequent sections. We begin by noting that the transformations

$$y = Y, \quad x = X - ct \quad (3.1)$$

introduce a frame of reference that moves with the wave phase speed (a Galileo transformation). This leads to the steady problem

$$(u - c)\frac{\partial u}{\partial x} + v\frac{\partial u}{\partial y} = -\frac{\partial p}{\partial x} + \frac{\partial^2 u}{\partial x^2} + \frac{\partial^2 u}{\partial y^2},$$
$$(u - c)\frac{\partial v}{\partial x} + v\frac{\partial v}{\partial y} = -\frac{\partial p}{\partial y} + \frac{\partial^2 v}{\partial x^2} + \frac{\partial^2 v}{\partial y^2}, \quad \frac{\partial u}{\partial x} + \frac{\partial v}{\partial y} = 0, \quad (3.2a–c)$$

subject to

$$u(1) = Re, \quad v(1) = 0, \quad u[y_L(x)] = 0, \quad v[y_L(x)] = -c\frac{\mathrm{d}y_L}{\mathrm{d}x}, \quad \frac{\partial p}{\partial x}\bigg|_{mean} = 0, \quad (3.2d–h)$$

with the position of the lower plate given by

$$y_L(x) = -1 + A\cos(\alpha x). \tag{3.2i}$$

The above system was solved numerically by first introducing a stream function ψ defined by

$$u = \frac{\partial \psi}{\partial y}, \quad v = -\frac{\partial \psi}{\partial x}, \tag{3.3a,b}$$

which automatically satisfies the continuity equation. The pressure is eliminated by taking the derivative of (3.2a) with respect to y and the derivative of (3.2b) with respect to x and subtracting the results. This reduces the flow problem to the following form:

$$\nabla^2(\nabla^2\psi) + c\frac{\partial}{\partial x}\nabla^2\psi = N_{uv} \quad \text{where } N_{uv} \equiv \frac{\partial}{\partial y}\left(\frac{\partial}{\partial x}(\widehat{uu}) + \frac{\partial}{\partial y}(\widehat{uv})\right) - \frac{\partial}{\partial x}\left(\frac{\partial}{\partial x}(\widehat{uv}) + \frac{\partial}{\partial y}(\widehat{vv})\right), \tag{3.4a}$$

$$y = 1: \ \frac{\partial \psi}{\partial y} = Re, \quad \frac{\partial \psi}{\partial x} = 0; \quad y = y_L(x): \ \frac{\partial \psi}{\partial y} = 0, \quad \frac{\partial \psi}{\partial x} = c\frac{\mathrm{d}y_L}{\mathrm{d}x}; \quad \left.\frac{\partial p}{\partial x}\right|_m = 0. \tag{3.4b–f}$$

The penultimate condition (3.4e) can be written in an alternative way by noting that variations in ψ along the lower plate can be expressed as

$$\mathrm{d}\psi_L = \left(\frac{\partial \psi}{\partial x}\,\mathrm{d}x + \frac{\partial \psi}{\partial y}\,\mathrm{d}y\right)\Big|_{y_L(x)} = c\frac{\mathrm{d}y_L}{\mathrm{d}x}\,\mathrm{d}x. \tag{3.5}$$

Integrating (3.5) along this plate yields

$$\psi_L(x) = c[y_L(x) - y_L(x_0)], \tag{3.6}$$

Where the constant of integration has been fixed by assuming that $\psi_L(x_0) = 0$, where x_0 is some arbitrary point along the plate. The stream function ψ is constant along the upper plate and its value can be determined from the pressure gradient constraint.

The system of equations (3.4)–(3.6) was solved to spectral accuracy by representing the unknowns in terms of Fourier expansions in the streamwise direction so that

$$\psi(x, y) = \sum_{n=-\infty}^{n=+\infty} \psi^{(n)}(y)\,\mathrm{e}^{\mathrm{i}n\alpha x} \tag{3.7}$$

for modal functions $\psi^{(n)}(y)$ to be determined. The boundary conditions at the upper plate are

$$y = 1: \ \frac{\mathrm{d}\psi^{(0)}}{\mathrm{d}y} = Re, \quad \frac{\mathrm{d}\psi^{(n)}}{\mathrm{d}y} = 0, \quad n \neq 0, \tag{3.8a,b}$$

with the constraint (3.8a) specifying the mean part of the streamwise velocity field; the requirement (3.8b) states that all the periodic components must be zero on the upper surface. While equations (3.8) provide explicit values for each modal function, they do not provide any coupling owing to the simple geometry. By way of contrast, the boundary conditions at the lower plate couple all the modes through the more complicated surface geometry. These boundary conditions were enforced using the concept of IBC.

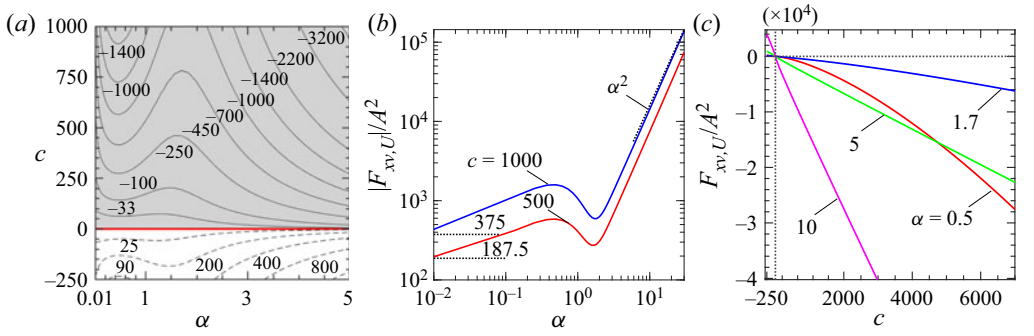

Figure 2. (*a*) Variations in the external force $F_{X,U}/A^2$ required to keep the upper plate stationary ($Re = 0$) as a function of α and c. The dividing red line shows the parameters for which $F_{X,U} = 0$ and the grey shading identifies those conditions for which $F_{X,U}$ is negative. (*b*) Some horizontal cuts taken through the results shown in (*a*) for the two wave speeds $c = 500$ and 1000. (*c*) Some vertical cuts taken through the results in (*a*) for the four wavenumbers $\alpha = 0.5$, 1.7, 5and 10.

The modal functions $\psi^{(n)}(y)$ were written as Chebyshev expansions while the flow boundary conditions were imposed as constraints. The overall algorithm is grid-less and is very flexible when changes in wave shape are of interest for it can be adjusted to account for multiple geometries with minimal user intervention. Our computations were carried out to ensure at least five-digit accuracy and this requirement dictated the choice of the number of Fourier modes and Chebyshev polynomials. The algorithm can be used to obtain results to machine accuracy if required. We have deliberately kept our description of the IBC strategy to a summary of the main points in the interest of brevity. Readers who desire a more leisurely and detailed discussion of the numerical method may consult with any of the papers by Szumbarski & Floryan (1999), Husain & Floryan (2008*a*,*b*, 2010) or Husain, Szumbarski & Floryan (2009).

3.1. *The peristaltic effect*

Before we embark on addressing the principal aim of the present study that concerns the reduction in the resistive forces, we quickly demonstrate the key properties of the peristaltic effect. We remark that vibrations imposed on the lower surface pump the fluid in the direction of the wave motion. The fluid movement exerts a shear stress on the upper plate which then requires an external force $F_{X,U}$ to keep it stationary. The sample of results presented in figure 2 demonstrates that $F_{X,U}$ increases with growth of α and c, which suggests that short, fast waves potentially provide the most effective form of pumping. Waves with $\alpha \approx 0.5$ provide a local maximum in $F_{X,U}$ which can be used to advantage in those applications where the creation of fast waves might prove difficult.

4. The reduction of resistance

When an external force is applied to the upper plate it accelerates and tends to pull the fluid along with it. Eventually an equilibrium is achieved in which the resistance generated by shear stresses balances the external force. The imposition of vibrations on the lower plate tends to force the fluid to move in the direction of the wave. This reduces the relative velocity of the fluid with respect to the upper plate and so lessens the shear that acts on that plate. It is likely that there will be a minimum wave velocity required for this effect to

come into play and that this least value will be a function of the plate velocity. We shall return to this issue a little later, but first probe the properties of the flow dynamics.

In an effort to understand these dynamics we look at the problem when the waves are long. We develop the detailed form of the long-wave structure in Appendix A and, for the purposes of the present discussion, borrow some of the key results derived there. In the limit $\alpha \to 0$ the streamwise velocity component has the form

$$u = \frac{1}{2}Re(\eta+1) - \frac{3}{4}Re\left[1 - \frac{4(4-A^2)}{(8+A^2)[2-A\ \cos(\xi)]}\right](1-\eta^2) \\ - c\frac{A}{2-A\ \cos(\xi)}\left[\frac{3}{2}\cos(\xi) - \frac{9A}{8+A^2}\right](1-\eta^2) + 0(\alpha), \tag{4.1}$$

where $\xi \equiv \alpha x$ and η is a transformed cross-slot coordinate so that the two plates are given by $\eta = \pm 1$.

This expression is comprised of three terms, the first being just the original Couette flow written in the new coordinates. The second term represents a Poiseuille-flow-type correction which we refer to as the 'groove effect'; we notice that this term does not depend on the wave phase speed but is a function of the groove amplitude so represents the effect of stationary grooves. The last term is proportional to the phase speed c so may be thought of as a 'wave effect'. We see that the groove effect is always negative; it leads to a retardation of the fluid and thus increases the resistance. On the other hand, the sign of the wave effect term depends on the direction of c; the wave must both travel in the flow direction and be sufficiently fast to overcome the groove effect. The interplay between these two effects can be explored by looking at the force required to maintain the movement of the upper plate. The component of this force that is attributable to vibrations can be written as

$$F_1 = \tilde{F}_0 - \frac{1}{2}Re + 0(\alpha^2) \\ = Re\left[\frac{4(2+A^2)}{(8+A^2)(4-A^2)^{1/2}} - \frac{1}{2}\right] - c\frac{6A^2}{(8+A^2)(4-A^2)^{1/2}} + 0(\alpha^2), \tag{4.2}$$

a result that is noted in equation (A23). The two terms here represent the groove and wave effects, respectively. Reducing the amplitude to zero ($A \to 0$) eliminates this force which is proportional to A^2 for small wave amplitudes. When the phase speed is made zero the grooves create an additional resistance ($F_1 > 0$) but reducing Re results in a peristaltic pumping within a slot with a fixed upper plate which produces a force acting on this plate in the direction of wave propagation. When waves are present and the upper plate is moving, waves propagating upstream ($c < 0$) increase the resistance encountered by the plate. The use of downstream-propagating waves decreases the resistance but only if the waves are fast enough – the pumping effect must be strong enough to overcome the effects of the grooves. We remark that vibrations with phase speed

$$c = Re\ A^{-2}\left[\frac{2}{3}(2+A^2) - \frac{1}{12}(8+A^2)(4-A^2)^{1/2}\right] \tag{4.3}$$

make F_1 zero and a further increase to

$$c = \frac{2}{3}Re\ A^{-2}(2+A^2) \tag{4.4}$$

brings the total force to zero. Then there is no need for an external force to maintain the specified plate velocity as the vibrations provide sufficient propulsion themselves. Of course, any further increase of c would require the use of a braking force to prevent plate acceleration.

A secondary quantity of interest is the flow rate driven by movement of the upper plate. Part of this flow can be attributed to the vibrations and equals

$$Q_{1,mean} = \tilde{Q}_{m,0} - Re + 0(\alpha^2) = c\frac{6A^2}{8+A^2} - Re\frac{3A^2}{8+A^2} + 0(\alpha^2). \tag{4.5}$$

We can see that the elimination of the grooves makes $Q_{1,mean}$ zero and that waves propagating upstream ($c < 0$) always reduce the flow rate. Waves propagating downstream help with propelling the fluid, but their phase speed needs to be at least $c = (1/2)Re$ to neutralize the groove effect.

This preliminary analysis already suggests that the wave speed relative to the fluid velocity may well prove to be important. It is not immediately clear how one should measure the fluid velocity unambiguously as it varies across the slot; consequently, we use the speed of the upper plate as a proxy for the fluid velocity. Thus far we have been concerned with long-wavelength modes and to assess other cases we need to resort to suitable numerical calculations.

4.1. *Vibration-induced flow modifications*

We have already noted that vibrations produce flow modifications that change the shear stress acting at, and hence the resistance experienced by, the upper plate. We now aim to characterize and understand some of the properties of this phenomenon and start by looking at how the flow is modified with changes in Re and c.

We start by plotting some representative instantaneous vector lines for the velocity modifications $\boldsymbol{u}_{mod} = \boldsymbol{u} - Re\boldsymbol{u}_0$ at a few typical wavenumbers α. The results shown in figure 3 suggest that the qualitative flow topologies appear to change little with variations in Re. Vibrations of a small wavenumber (figure 3*a*,*d*,*g*,*j*) lead to a sloshing pattern with forward movement around the wave troughs and backward movement near the crests. In contrast, at a large wavenumber $\alpha = 10$ (figure 3*c*,*f*,*i*,*l*) a boundary layer is formed near the vibrating plate and a uniform flow persists above it; we refer to this as a moving-wall regime. Patterns at intermediate values of α appear as a hybrid between the sloshing and the moving-wall structures.

We provide more insight into the velocity modifications by plotting the profiles of this quantity at four streamwise locations. In figure 4(*a*,*d*,*g*,*j*) we see that at a small wavenumber the modifications are of appreciable size over the entire width of the slot. In contrast, in the case of short waves (figure 4*c*,*f*,*i*,*l*) the modifications have a somewhat involved x-dependent form near the vibrating plate, but they smoothly morph into an almost x-independent, Couette-like flow outside the boundary layer. These velocity distributions are only slightly modified by variations in Re and their profiles are hardly affected by changes in c although their magnitude is roughly proportional to c.

It is instructive to discuss further the flow modifications at a high wavenumber as they demonstrate explicitly the process of transferring wave propulsion from the lower to the upper plate. Vibrations tend to pump the fluid to the right within the boundary layer whose edge acts rather like a moving wall with an apparent velocity U_{app}. An estimate of U_{app} can be obtained by looking at the value of u_{mod} at the edge of the boundary layer (figure 5*a*) and it seems that U_{app} increases proportional to α^2 as $\alpha \to \infty$ (figure 5*b*,*c*).

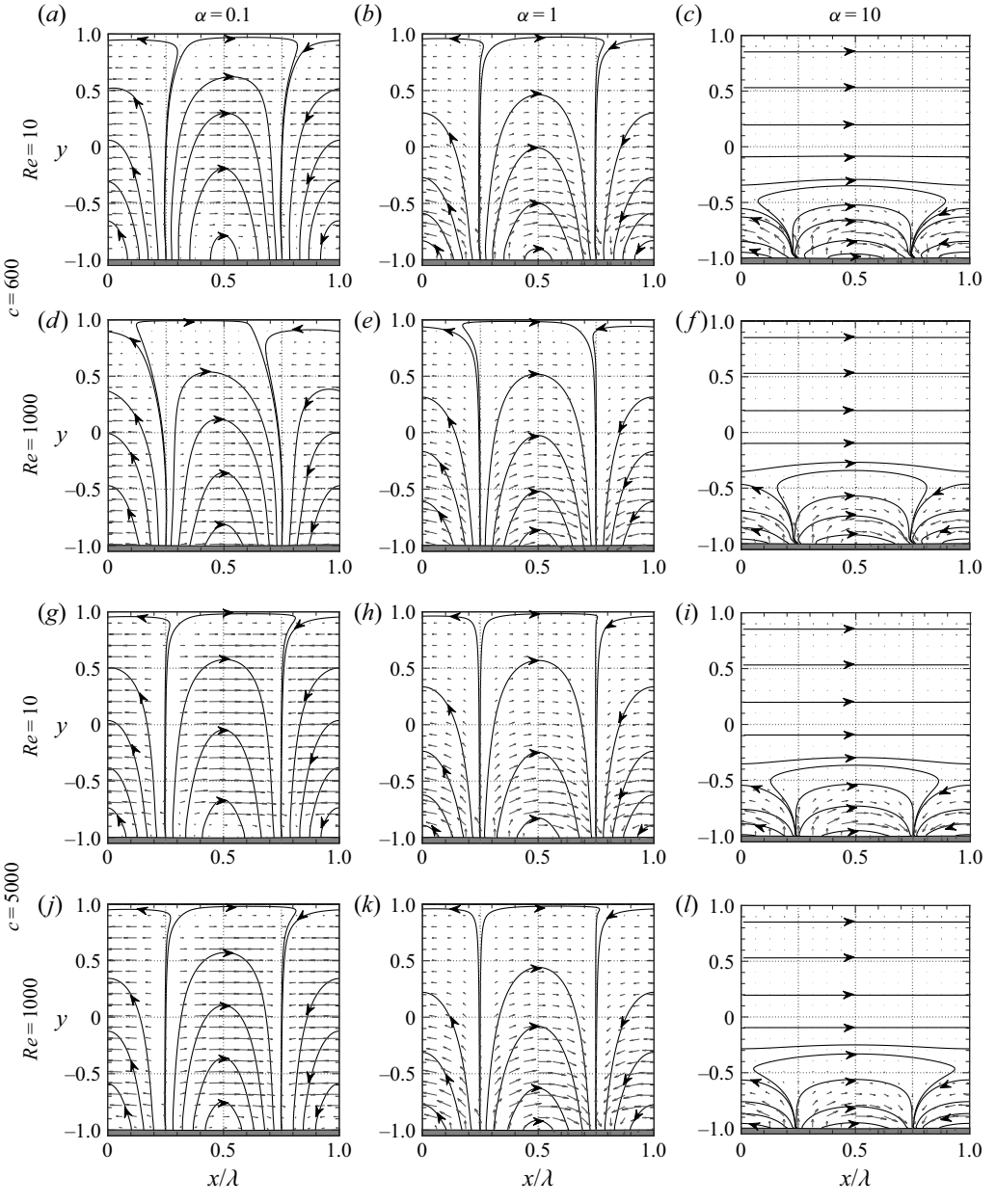

Figure 3. Distributions of the modified streamwise flow field for groove amplitude $A = 0.0025$. The wavenumber $\alpha = 0.1$ (*a*,*d*,*g*,*j*), 1 (*b*,*e*,*h*,*k*) and 10 (*c*,*f*,*i*,*l*) and the results are shown for two wave speeds $c = 600$ and 5000 and two Reynolds numbers $Re = 10$ and 1000.

The flow outside the boundary layer is essentially of Couette type driven by this moving wall in the direction of wave motion and this flow is responsible for transferring the vibration-generated propulsion to the upper plate.

We now look in detail at the resistance experienced by the upper plate. In order to simplify the presentation, we divide the results into three parts according to the speed of the upper plate. We start with relatively slow motions.

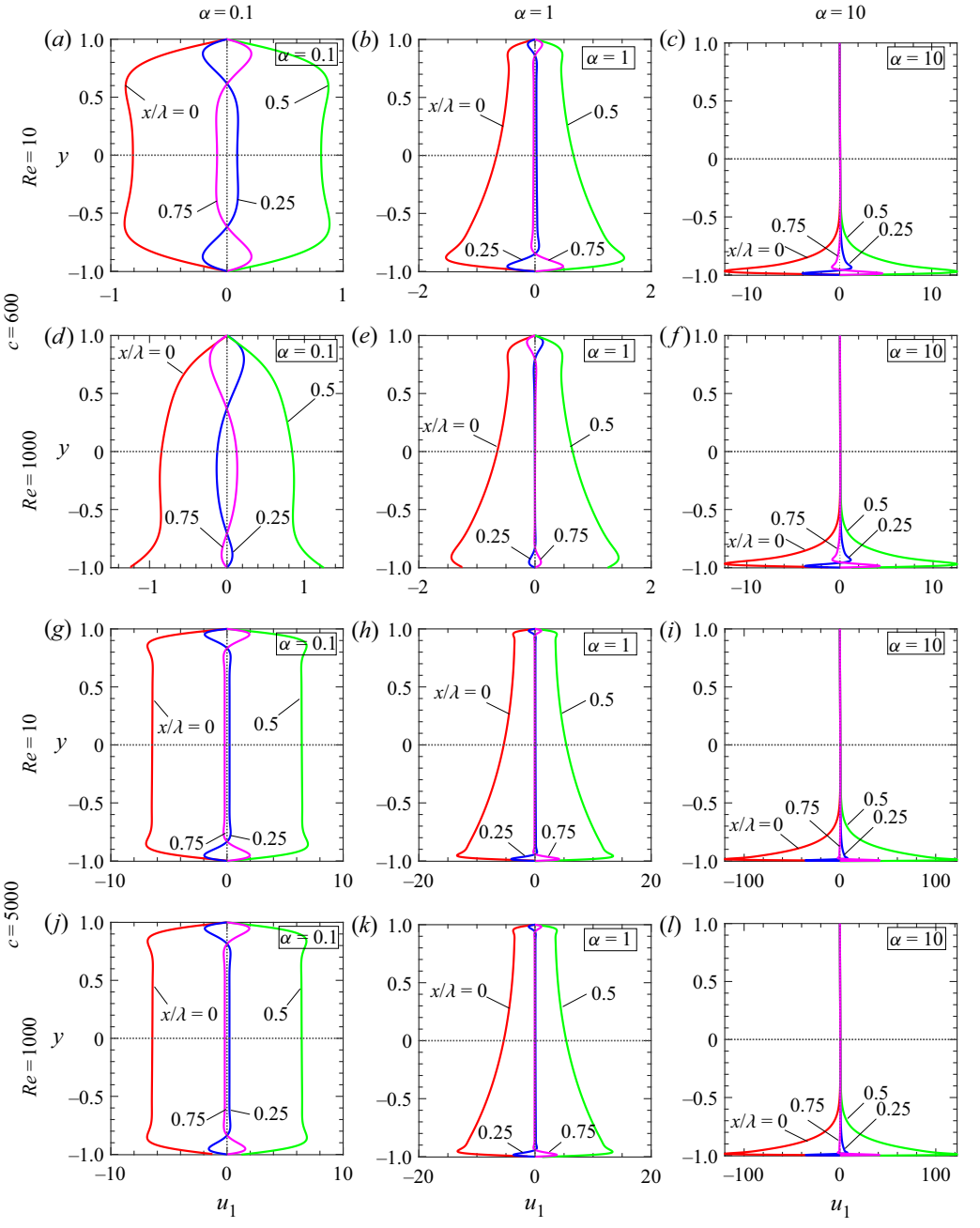

Figure 4. The distributions of the velocity modification at the four streamwise locations $x/\lambda = 0, 0.25, 0.5, 0.75$ when the groove amplitude $A = 0.0025$. The wavenumber $\alpha = 0.1$ (*a*,*d*,*g*,*j*), 1 (*b*,*e*,*h*,*k*) and 10 (*c*,*f*,*i*,*l*) and the results are shown for two wave speeds $c = 600$ and 5000 and two Reynolds numbers $Re = 10$ and 1000.

5. Slow plate movement ($Re \leq 100$)

The fact that the upper plate moves breaks the symmetry that would otherwise be present between waves that move to the left or to the right. Forward-moving waves, that is, those

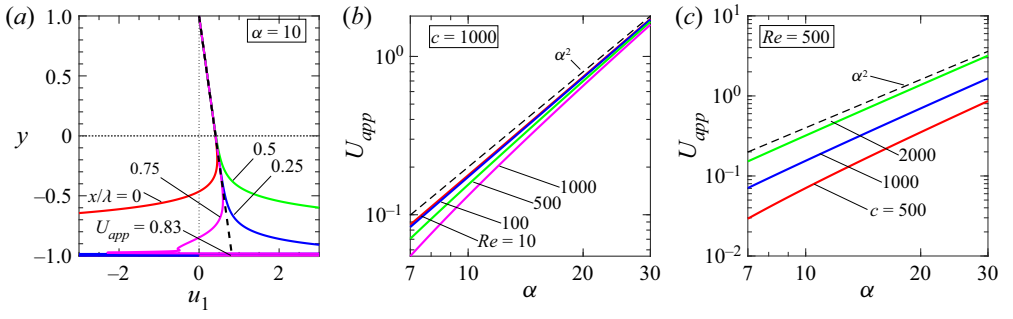

Figure 5. (*a*) Zoomed-in picture of the velocity distribution for $\alpha = Re = 10$ and $c = 5000$. Plots of U_{app} as a function of α (*b*) when $c = 1000$ for various Re and (*c*) when $Re = 500$ for various c. In all cases groove amplitude $A = 0.0025$.

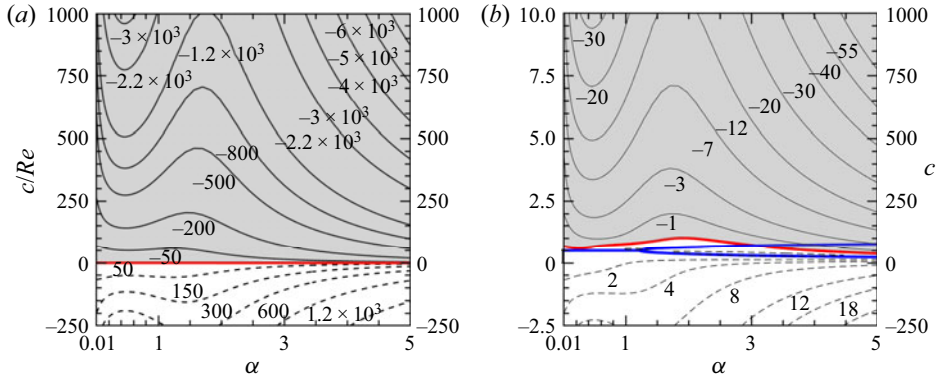

Figure 6. Variations in the normalized force correction $F_{norm} = F_1/ReF_0A^2$ as a function of α and c when (*a*) $Re = 1$ and (*b*) $Re = 100$. The grey shading indicates negative values while the red line shows those values that give $F_1 = 0$. Zones between the blue lines in (*b*) denote the range of natural frequencies of the Orr–Sommerfeld modes (see Appendix B).

that move in the same direction as the plate, may well reduce the necessary pulling force required to maintain motion, while backward-moving waves are more likely to increase this force. This speculation is confirmed by the results shown in figure 6.

If the waves move more slowly than the fluid, the plate modifications associated with vibrations play a role akin to that of surface roughness. By way of contrast, if the waves are quicker than the fluid this activates peristaltic pumping which decreases the external pulling force. While these comments are somewhat qualitative in nature, we can be more precise as to the divide between slow and fast waves in the case of long wavelengths. The reader is reminded that in the case $\alpha \to 0$ the form of the force correction F_1 is given by (4.2), and then since this quantity needs to be negative to achieve a force reduction, we can determine the phase speed c_b which separates the 'faster' and 'slower' waves as

$$c_b = \frac{Re}{1+Re}(6A^2)^{-1}\left[4 + A^2 - \frac{1}{2}(8+A^2)(4-A^2)^{1/2}\right]. \tag{5.1}$$

The situation is somewhat more involved for waves with $\alpha = 0(1)$. Now an increase in the upper plate velocity Re leads to a discernible dependence of c_b on α; if we examine the red dividing lines in figure 6 then if $Re = 1$ the value of c_b appears to be virtually

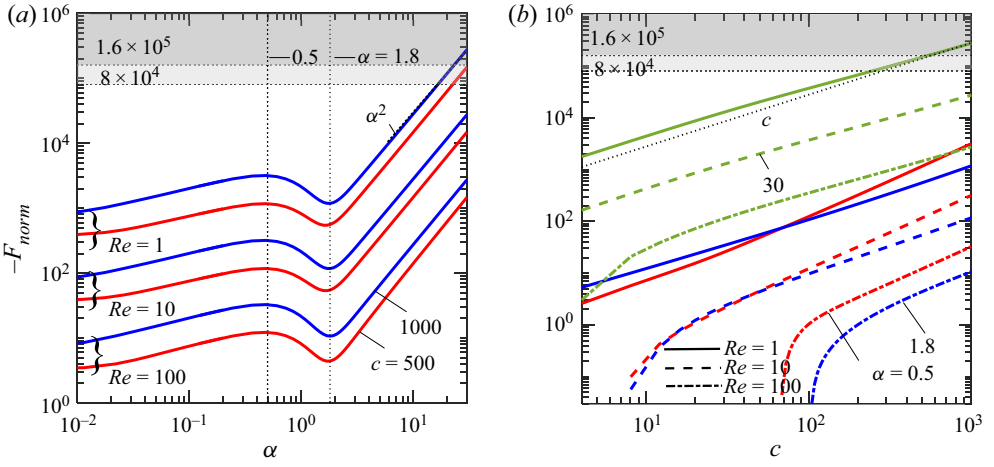

Figure 7. The variations of the normalized force correction $F_{norm} = F_1/ReF_0A^2$. (*a*) Force as a function of α for the three Reynolds numbers $Re = 1$, 10 and 100 and the two speeds $c = 500$ and 1000. The dark shading identifies conditions which require an external braking force while the lighter shading shows those parameters that lead to at least a 50 % reduction in the pulling force. (*b*) Force as a function of c for the same three values of Re and the three wavenumbers $\alpha = 0.5$ (red), 1.8 (blue) and 30 (green).

independent of α but this is certainly not the case in figure 6(*b*) for which $Re = 100$. The size of the resistance reduction correlates reasonably well with the strength of peristaltic effect discussed earlier in the sense that fast, short waves appear to be the most effective. We also point out that there is a local maximum in F_1 near $\alpha \approx 0.5$ which suggests that if high-velocity waves cannot easily be created, then a good compromise might be achievable using modes of this wavenumber.

More detailed information concerning the dependence of F_1 on the various parameters can be obtained by looking at the results at a fixed value of c. The results shown in figure 7(*a*) reveal that F_1 varies nonmonotonically with α and this quantity has turning points near $\alpha \approx 0.5$ and $\alpha \approx 1.8$. The effectiveness of the vibrations increases as Re falls since momentum inserted at the lower plate is transferred to the upper plate through viscous effects. A reduction in Re can be interpreted as a shortening of the distance between the plates which naturally increases the effectiveness of shear stresses. Sufficiently short-wavelength, fast vibrations can eliminate the required external force completely and may even lead to situations when this force changes direction so that a braking force is needed otherwise the plate would accelerate. If we examine the form of the force F_1 as a function of c at a fixed value of α we obtain the results sketched in figure 7(*b*). We see that F_1 increases with c in a somewhat complicated way when Re is relatively small but at higher values the rise in F_1 becomes almost exactly proportional to c.

We can put a fresh interpretation on the role played by the wavenumber α with reference to the earlier results shown in figures 3 and 4. There we identified three distinct regimes: at small wavenumbers we have a sloshing motion, at large wavenumbers a moving-wall motion and there is an intermediate transitional regime between these extremes. The characteristics of the flow affect the shear exerted on the upper plate, which is the principal factor in achieving the desired resistance reduction. Different processes lead to shear reduction in the sloshing and moving-wall scenarios while the transition regime can

be viewed as hybrid of the two; the existence of the three separate cases is evident in figure 7(*a*).

The underlying Couette flow possesses a collection of natural frequencies which can be determined by methods outlined in Appendix B. These frequencies are associated with travelling waves whose phase speeds C_r are known to lie between 0 and Re (Schmid & Henningson 2001). Tighter bounds on these speeds have been determined numerically for each α and are superimposed on figure 6. These waves are highly attenuated and can persist only with a continuous addition of energy. It is possible that the vibrations of the lower plate could provoke near-resonances with the natural frequencies and could conceivably drive instabilities (Floryan, Szumbarski & Wu 2002). The fact that the phase speed C_r of the travelling cannot exceed Re suggests that our imposed vibration waves might be distinguished depending on whether they are fast ($c > Re$) or slow ($0 < c < Re$); clearly fast waves cannot interact with the natural frequencies. As Re increases so the natural waves become less attenuated and can interact more effectively with the vibrations thereby restricting the opportunities for resistance reduction. The results displayed in figure 6(*a*) for $Re = 1$ do not show interactions as the natural modes are highly attenuated but these interactions become noticeable by the stage $Re = 100$ (see figure 6*b*). We remark that the natural frequencies of the reference Couette flow provide only a guideline as to possible interactions with the vibration modes. This is because the flow modified by vibrations is likely to possess a much more complex spectrum of natural frequencies as evidenced by analogous calculations pertaining to Poiseuille flow in a grooved channel (Asai & Floryan 2006; Floryan 2007). To the best of our knowledge the stability analysis of Couette flow modified by vibrations has yet to be examined.

5.1. *A simple energy budget*

Next, we examine the various energy fluxes in the system as the imposition of vibrations requires an expenditure of energy. The energy fluxes are determined by multiplying the x-momentum equation by u, the y-momentum equation by v, adding them together and then integrating over the control volume which extends between the plates in the y direction and over one wavelength in the x direction (Bewley 2009; Jiao & Floryan 2021). The resulting balance has the form

$$\int_0^\lambda \int_{y_L}^1 \left(u^2 \frac{\partial u}{\partial x} + uv \frac{\partial u}{\partial y} + uv \frac{\partial v}{\partial x} + v^2 \frac{\partial v}{\partial x} \right) \mathrm{d}y \, \mathrm{d}x$$
$$= -\int_0^\lambda \int_{y_L}^1 \left(u \frac{\partial p}{\partial x} + v \frac{\partial p}{\partial y} \right) \mathrm{d}y \, \mathrm{d}x + \int_0^\lambda \int_{y_L}^1 \left(u \frac{\partial^2 u}{\partial x^2} + u \frac{\partial^2 u}{\partial y^2} + v \frac{\partial^2 v}{\partial x^2} + v \frac{\partial^2 v}{\partial y^2} \right) \mathrm{d}y \, \mathrm{d}x. \tag{5.2}$$

We can write this result in a more convenient way by integrating each term by parts, simplifying using continuity and then imposing the requisite streamwise periodicity properties. This process leads to the result that

$$Re\lambda^{-1} \int_0^\lambda \left(\frac{\partial u}{\partial y} \right)_{y=1} \mathrm{d}x = P_\varepsilon - P_{wv} - P_k - P_{wp}, \tag{5.3a}$$

where the left-hand side of this balance denotes the external power (per unit length of the slot) required to drive the upper plate. The four terms on the right-hand side are defined by

$$P_\varepsilon \equiv \lambda^{-1}\int_0^\lambda\int_{-1}^1\left[\left(\frac{\partial u}{\partial x}\right)^2+\left(\frac{\partial u}{\partial y}\right)^2+\left(\frac{\partial v}{\partial x}\right)^2+\left(\frac{\partial v}{\partial y}\right)^2\right]\mathrm{d}y\,\mathrm{d}x,$$

$$P_{wv} \equiv \lambda^{-1}\int_0^\lambda\left(v\frac{\partial u}{\partial x}\right)_{y=y_L}\mathrm{d}x, \qquad (5.3b,c)$$

$$P_k \equiv \lambda^{-1}\int_0^\lambda\left[v\left(\frac{1}{2}v^2\right)\right]_{y=y_L}\mathrm{d}x \quad \text{and} \quad P_{wp} \equiv \lambda^{-1}\int_0^\lambda (vp)_{y=y_L}\,\mathrm{d}x, \qquad (5.3d,e)$$

with P_ε representing the rate of energy dissipation, P_{wv} denoting the rate of work done by viscous forces at the vibrating plate, P_k representing the rate of injection of kinetic energy into the flow at the vibrating plate and P_{wp} standing for the rate of work done by pressure forces at the vibrating plate. We point out that $P_k \equiv 0$ for sinusoidal vibrations and that the application of this balance to a smooth slot leads to the simple expression for the external power, i.e. $\frac{1}{2}Re^2$ $(= P_\varepsilon)$ with P_{wv}, P_k and P_{wp} all zero. This enables us to derive an expression for the change in the external energy required to generate the vibrations which is given by $P_{wv} + P_{wp}$. The introduction of vibrations changes the velocity field thereby increasing dissipation by $\Delta Dis = P_\varepsilon - \frac{1}{2}Re^2$ and moderating the external power ΔP_{we} $(= \Delta Dis - P_{wv} - P_{wp})$ necessary to maintain the plate motion. Rearranging terms in (5.3*a*) we get

$$P_\varepsilon = Re\,\lambda^{-1}\int_0^\lambda\left(\frac{\partial u}{\partial y}\right)_{y=1}\mathrm{d}x + P_{wv} + P_k + P_{wp}, \qquad (5.3f)$$

which shows how to reduce dissipation to achieve net energy savings. Sample forms of the pressure work term P_{wp} are shown in figure 8(*a*,*e*) as a function of α and c, and equivalent results for P_{wv} and the dissipation ΔDis are presented in figures 8(*b*,*f*) and 8(*c*,*g*), respectively. Inspection of the form of ΔP_{wr} required by the upper plate suggests that a reduction in power requirements is necessary for sufficiently fast forward-moving waves with larger reductions obtained for shorter waves (see figure 8*d*,*h*). It would seem that P_{wp} represents the dominant energy flux and most of it is consumed by the increase of dissipation with only small fraction that can be ascribed to a reduction in the power required to maintain the plate movement. So, it can be inferred that the vibration configurations considered within the scope of this analysis do not produce net energy saving.

6. Intermediate plate speeds ($100 < Re < 1000$)

We have seen that an increase in the plate velocity much above about $Re = 100$ requires faster waves to achieve a reasonable reduction in the resistance. Once we reach this regime, the waves may approach a near resonance with the natural flow frequencies and this plausibly could result in a significant deterioration of the system performance. This problem can be circumvented by working with waves that are faster than the plate velocity; we have already noted that such waves will then be outside the range within which the natural flow frequencies must lie. This allows us to divide the waves into two classes: waves with $c > Re$ are subsequently referred to as supercritical as they cannot interact with

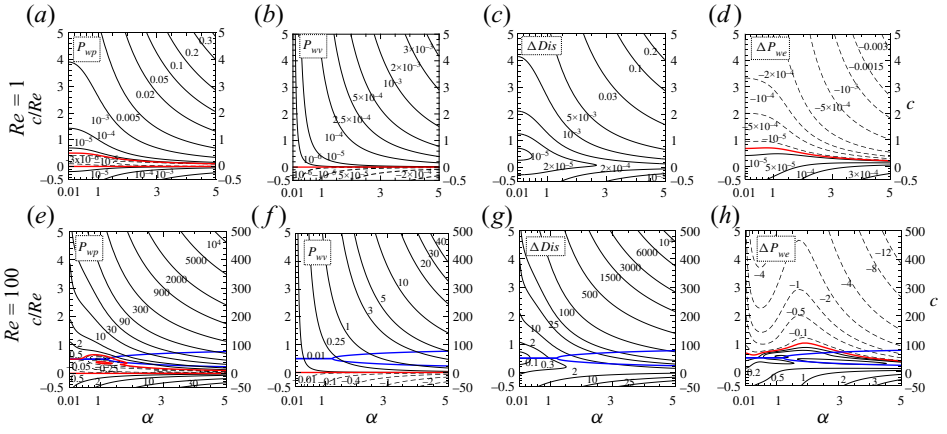

Figure 8. Components of the energy budget at the two Reynolds numbers $Re = 1$ and $Re = 100$. Work done (a,e) by pressure at the lower plate P_{wp} and (b,f) by viscous forces at the lower plate P_{wv}. (c,g) The increase of dissipation above its reference value ΔDis and (d,h) the change in power ΔP_{we} required to drive the upper plate. All results correspond to a groove amplitude $A = 0.01$; solid (dashed) lines denote positive (negative) values. The red lines indicate zero values and the zones between the blue lines shows the range of natural frequencies of the Orr–Sommerfeld modes.

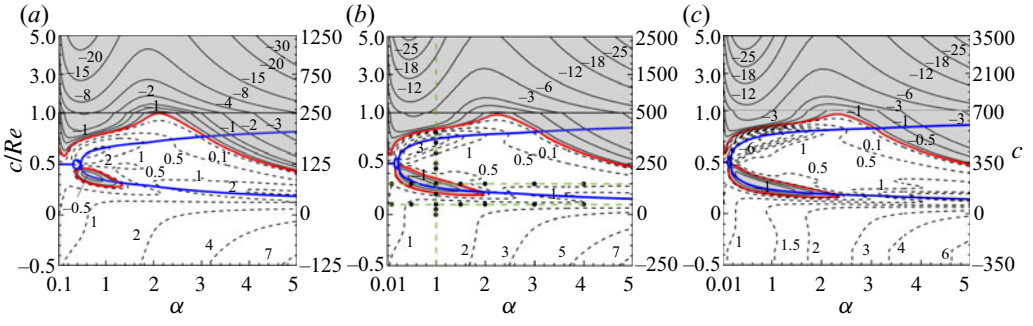

Figure 9. The variations in the normalized force correction $F_{norm} = F_1/ReF_0A^2$ as a function of α and c for the three Reynolds numbers (a) $Re = 250$, (b) $Re = 500$ and (c) $Re = 700$. The grey shading indicates regions of parameter space corresponding to a reduction in resistance and the red lines mark conditions for which $F_1 = 0$. The zones between the blue lines denotes the range of natural frequencies of the Orr–Sommerfeld modes. The black dots identify conditions used in the later figures 12–16.

the natural frequencies; those waves with $0 < c < Re$ will be deemed to be subcritical and interaction may be possible.

The form of F_1 as a function of c and α is illustrated in figure 9. Supercritical waves appear to reduce the magnitude of F_1 although the functional from of $F_1(\alpha, c)$ is very reminiscent of the results found for the slow-plate problem. In contrast, subcritical waves lead to a complex structure in which zones of resistance reduction are interspersed with regions of parameter space in which the resistance increases; this is qualitatively different behaviour from that found at smaller Re.

The subcritical waves generally lead to an increase in the resistance. A reduction in resistance may be possible using waves with velocities towards the upper limit of the subcritical range. The cross-over point where there is no change in the resistance ($F_1 = 0$) is a function of α and is delineated by the red lines in figure 9. There are also small isolated

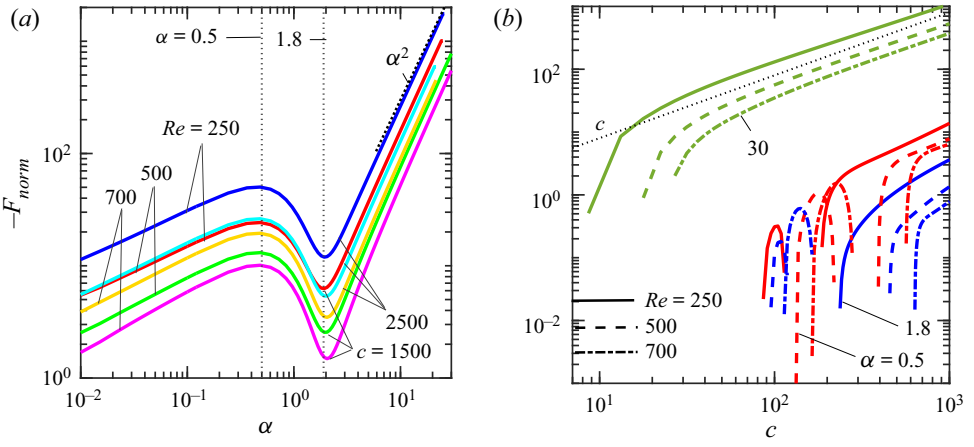

Figure 10. Variations of the normalized force correction $F_{norm} = F_1/ReF_0A^2$. (*a*) The correction as a function of α for the Reynolds numbers $Re = 250$, 500 and 700 and wave speeds $c = 1500$ and 2500. (*b*) The correction as a function of c for the same Reynolds numbers and wavenumbers $\alpha = 0.5$, 1.8 and 30.

regions of negative F_1 centred near $\alpha \approx 0.8$ and $c/Re \approx 0.3$ and these zones identify additional conditions under which force reduction is possible. These regions appear to expand as Re increases. There are also other regions of parameter space in which the opposite effect occurs and an anomalously large increase in resistance is seen. These zones seem to be centred around $\alpha \approx 0.8$ and $c/Re \approx 0.7$ and, again, they spread out with an increase of Re with most of the expansion occurring in the α direction.

Cuts taken through the contour plots at a fixed c within the force-reducing zone are shown in figure 10(*a*). These results demonstrate that F_1 varies as function of α in a somewhat complicated fashion. We see that the magnitude of the correction force has a local maximum near $\alpha \approx 0.5$ and a local minimum around $\alpha \approx 1.8$; this is not dissimilar to what was seen for slow plate movements (figure 7). The effectiveness of the vibrations diminishes with Re, but this can be compensated for by a concomitant increase in the wave speed. The influence of short waves appears to grow approximately proportional to α^2; see figure 10(*a*). The form of the correction force as a function of c at fixed α is shown in figure 10(*b*). We conclude that the magnitude of F_1 increases in a non-simple manner for slow (subcritical) waves with this growth becoming nearly proportional to c for supercritical modes.

Supercritical waves are associated with energy fluxes whose variations with c and α are qualitatively not dissimilar to those seen relating to the slow plate movements (figures 8 and 11). Subcritical waves lead to intricate and quite different variations as illustrated in figure 11 – we shall look at these in some detail. Vibrations do the work for waves with velocities near the upper limit of the subcritical range, with the borderline $P_{wp} = 0$ being a function of α and being marked red in figure 11(*a*). There are small parameter regions where $P_{wp} > 0$ and these are centred around $\alpha \approx 0.8$ where the vibrations also do the work. The flow appears to perform most of the work in the remaining part of the parameter space displayed in figure 11(*a*) with the maximum of this effort occurring near $\alpha \approx 0.8$, $c \approx 0.7$. Variations in the power required to maintain the plate movement show similar areas of decreased external power as well as regions where a reduction in this power is possible (figure 11*d*). The variations in the viscous work are quite regular (figure 11*b*) with this work increasing with both c and α. Rapid changes in the dissipation (see figure 11*c*) appear at those parts of the parameter conditions corresponding to the islands identified

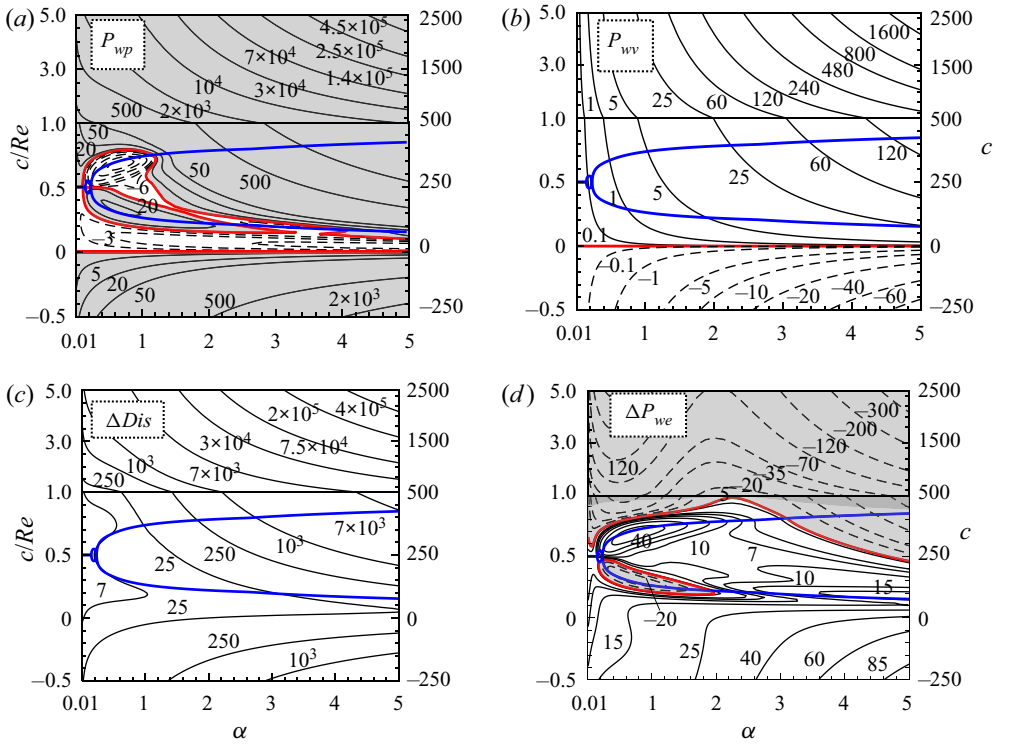

Figure 11. (*a*) The work done by the pressure at the lower plate P_{wp} and (*b*) the work done by viscous forces at the lower plate P_{wv}. (*c*) The increase in dissipation above its reference value and (*d*) the change in power ΔP_{we} required to drive the upper plate. Solid (dashed) lines represent positive (negative) values. The red lines denote zero contours and the zones between the blue lines indicate the range of natural frequencies of the Orr–Sommerfeld modes. All results given are for $Re = 500$ and $A = 0.01$. The grey shading identifies the region of $P_{wp} > 0$ in (*a*) and $\Delta P_{we} < 0$ in (*d*).

in figure 11(*a*); outside this zone dissipation increases monotonically with an increase of both c and α. There is no net energy savings associated with such waves.

We next look in detail at the variations in the various forces and energies as functions of the wave speed and focus on the case $Re = 500$ for definiteness. We summarize the main findings in figure 12. The key quantities, being the pressure component of the force on the lower plate $F_{Xp,L}$ (2.11), the work done by the pressure at the lower plate P_{wp} (5.3), the force correction F_1 and the change in power ΔP_{we}, change in smooth monotonic ways for supercritical waves but behave in a rather complicated manner when the waves are subcritical. These complications simplify somewhat for shorter waves as then the corresponding natural frequencies are highly attenuated.

To probe further into the system dynamics for subcritical waves, we reconfigure the data from figure 12 and discuss the results for fixed values of the wavenumber α; see figure 13. The results confirm significant intricacies in the flow response for long waves. The waves with $\alpha = 0.5$ in figure 13(*a*) include a cross-section that cuts through an island of decreased F_1 in figure 9(*b*) as well as a zone of significant increase in F_1. This cut also contains regions of positive and negative pressure work (figure 11*a*). Our results demonstrate a change in the direction of the pressure force as c increases; this force opposes the fluid movement for $0 < c < 0.25\,Re$, then weakly encourages the fluid movement and then opposes the fluid movement again when $0.5\,Re < c < 0.75\,Re$.

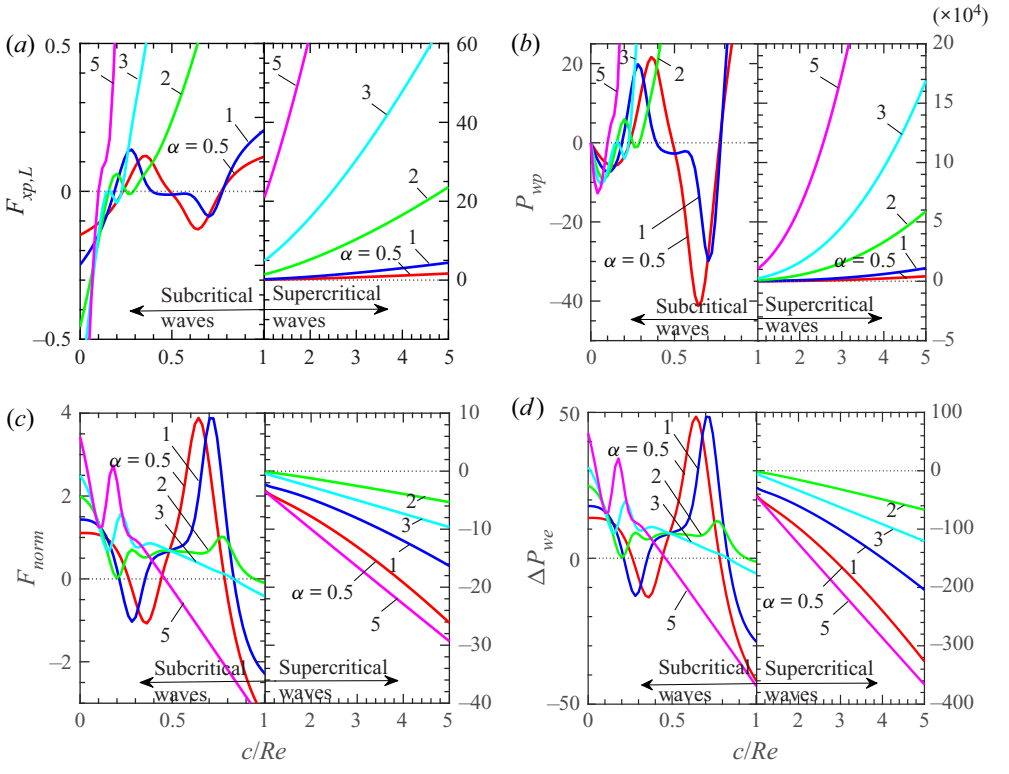

Figure 12. (*a*) The variation in the x component of the pressure force $F_{Xp,L}$ that acts on the fluid at the lower plate. (*b*) The pressure work done at the lower plate P_{wp}; (*c*) the normalized force correction $F_{norm} = F_1/ReF_0A^2$ and (*d*) the change of the power ΔP_{we} required to drive the upper plate. All results relate to $Re = 500$, a groove amplitude $A = 0.01$ and the five wavenumbers $\alpha = 0.5$, 1, 2, 3 and 5.

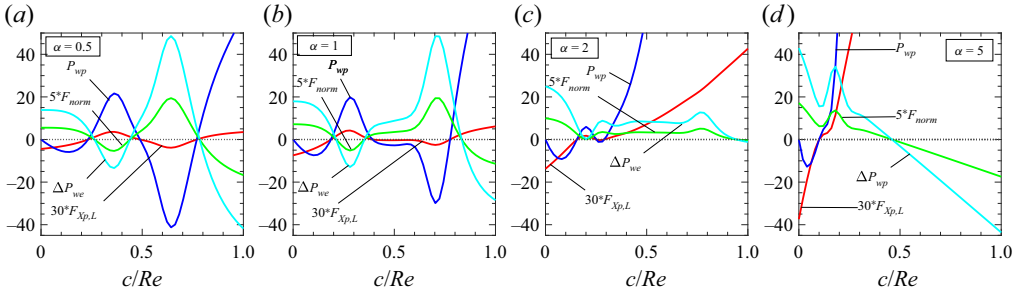

Figure 13. The x component of the pressure force $F_{Xp,L}$, the pressure work done at the lower plate P_{wp}, the normalized force correction $F_{norm} = F_1/ReF_0A^2$ and the change of the power ΔP_{we} required to drive the upper plate all plotted as functions of c/Re. All results relate to $Re = 500$, a groove amplitude $A = 0.01$ and prescribed wavenumbers $\alpha =$ (*a*) 0.5, (*b*) 1, (*c*) 2 and (*d*) 5.

Any further increase in c just results in an ever-increasing force that promotes the fluid movement. The external force applied to the upper plate increases when the pressure force opposes the fluid movement and decreases when it is supporting (figures 12*c* and 13*a*) and changes in the external power display similar variation (figures 12*d* and 13*a*).

A slight increase in the wavenumber to $\alpha = 1$ largely preserves the qualitative character of variations of all the quantities depicted in figure 13(*a*). A further increase to $\alpha = 2$ decreases the amplitude of oscillation in F_1 and ΔP_{we} almost tenfold (figure 13*c*) and growth in both P_{wp} and $F_{Xp,L}$ is noted once $c > 0.4Re$. With $\alpha = 5$ (figure 13*d*) the growing trend in P_{wp} and $F_{Xp,L}$ sets it at smaller values of c.

To explain the observed variations in forces and power, we present in figure 14 streamwise profiles of the pressure at the lower plate p_L together with the x component of the pressure force $\sigma_{xp,L}$. We fix the wavenumber $\alpha = 1$ and consider two ranges of wave speed. When $c = 0$ the groove is stationary, and the minimum pressure occurs slightly downstream from the peaks with the maximum positioned slightly near the troughs. The distribution of the force $\sigma_{xp,L}$ shows that it is directed upstream and so is opposing the fluid movement. As the wave speed increases, so the motion drives the pressure minimum downstream with the size of the pressure variations remaining virtually unchanged until $c \approx 0.1Re$ but these tend to grow thereafter with the greatest amplitude occurring when $c \approx 0.3Re$. The evolution of $\sigma_{xp,L}$ follows a broadly similar pattern as illustrated in figure 14(*c*,*d*). Once the wave speed exceeds $c \approx 0.45Re$ the pressure distribution shifts by a half-period with respect to the wave and any further increase in c leads only to an increase in the pressure amplitude but with no change in the position of the pressure peaks. The profile of $\sigma_{xp,L}$ also shows the formation of a regular pattern characterized by an increasing amplitude of oscillation. We saw in figure 13(*b*) that for $Re = 500$ and $\alpha = 1$ there are ranges of c over which the pressure force opposes fluid movement interspersed with regimes over which it promotes it. This suggests that it is the combination of the size of pressure variations in conjunction with the position of the pressure pattern relative to the wave which together determine whether the vibration-created force reduces or increases the movement resistance.

To complement the results displayed in figure 14 we investigate how the properties of p_L and $\sigma_{xp,L}$ behave as functions of the wavenumber for a fixed wave speed c. We chose to focus on the case $c = 0.3Re$ and this is motivated by the observation that this cross-section in figure 9(*b*) includes regions in which the overall resistance grows and others in which it decreases. It is seen that the pressure maxima for the long waves are located near the wave crests and minima near the troughs. There is a half-wavelength phase shift in the pressure distribution when α increases much beyond about $\alpha = 1.5$ and any further increase in α leads only to an increase in the size of the pressure variations. The forms of $\sigma_{xp,L}$ illustrate the effects of both a phase change and a monotonic increase of amplitude when α increases beyond $\alpha = 1.5$. We remark that the results summarized in figure 9(*b*) suggest that when $Re = 500$ and $c = 0.3Re$, the force correction is positive for longish ($\alpha < 0.33$) or shortish ($\alpha > 1.35$) waves but is negative otherwise. At the lower speed $c = 0.1Re$ we note from figure 9(*b*) that the resistance always increases irrespective of the value of α. At this relatively slow speed the results in figure 15 demonstrate that the maximum in the surface pressure when α is small tends to be located near wave troughs but it shifts downstream towards the crests as α increases. There is no discernible phase shift such as that associated with the waves at the higher speed $c = 0.3\ Re$. We also note that the distribution of $\sigma_{xp,L}$ is characterized by a large amplitude which seems to increase with α up to the point when $\alpha \approx 1$ and that the pressure force always opposes the fluid movement.

7. Fast plate speeds ($Re \geq 1000$)

In order to explore the characteristics of the flow when the upper plate moves much more quickly, we focus on the two Reynolds numbers $Re = 1000$ and 2000. We find that the overall properties of the force correction term F_1 remain somewhat like those already

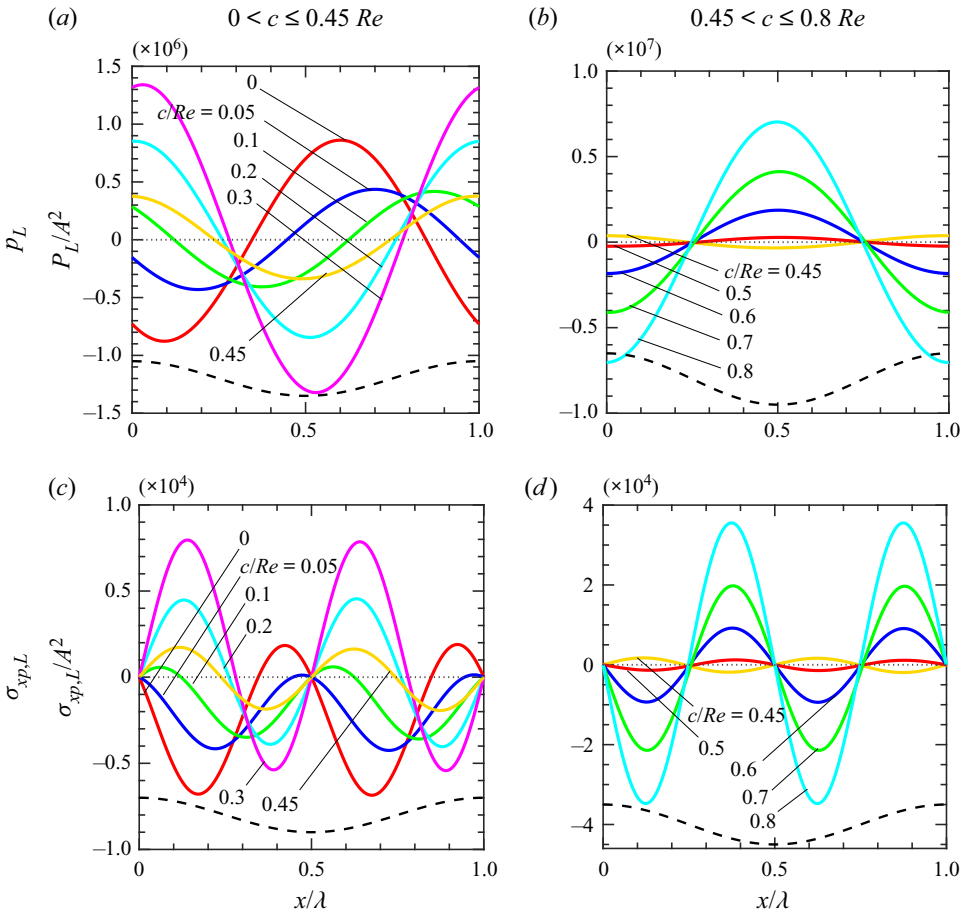

Figure 14. The distributions of the surface pressure p_L at the lower plate (*a*,*b*) and the x component of the pressure force acting on the fluid at the lower plate $\sigma_{xp,L}$ (*c*,*d*). All results are for $\alpha = 1$, $Re = 500$, $A = 0.01$.

seen in as much that short, fast waves seem to be the most effective in reducing the resistance. It, however, becomes increasingly difficult to achieve a significant reduction as high wave speeds are required to achieve supercritical performance. This brings into play the importance of understanding the flow modulations caused by subcritical waves which, it should be stressed, though slower than the speed of the upper plate, are by no means slow in any absolute sense. The complexities of the system response to such waves are illustrated in figure 16 which shows islands of reduced values of F_1 surrounded by regions in which the resistance increases.

If we look at the results summarized figure 16 but at a fixed value of c that lies solidly in the region where $F_1 < 0$ we obtain profiles of the type shown in figure 17(*a*). It is clear that F_1 has a local maximum around $\alpha \approx 0.5$, not dissimilar to the case of smaller Re (see figures 7 and 10), but the local minimum moves to $\alpha \approx 2.2$. The overall effectiveness of vibrations decreases but this can be compensated for by reducing the wavelength and increasing the phase speed. Results at a fixed value of α, see figure 17(*b*), show that F_1 increases in a somewhat intricate way for slow waves but the growth becomes nearly proportional to c for sufficiently fast modes.

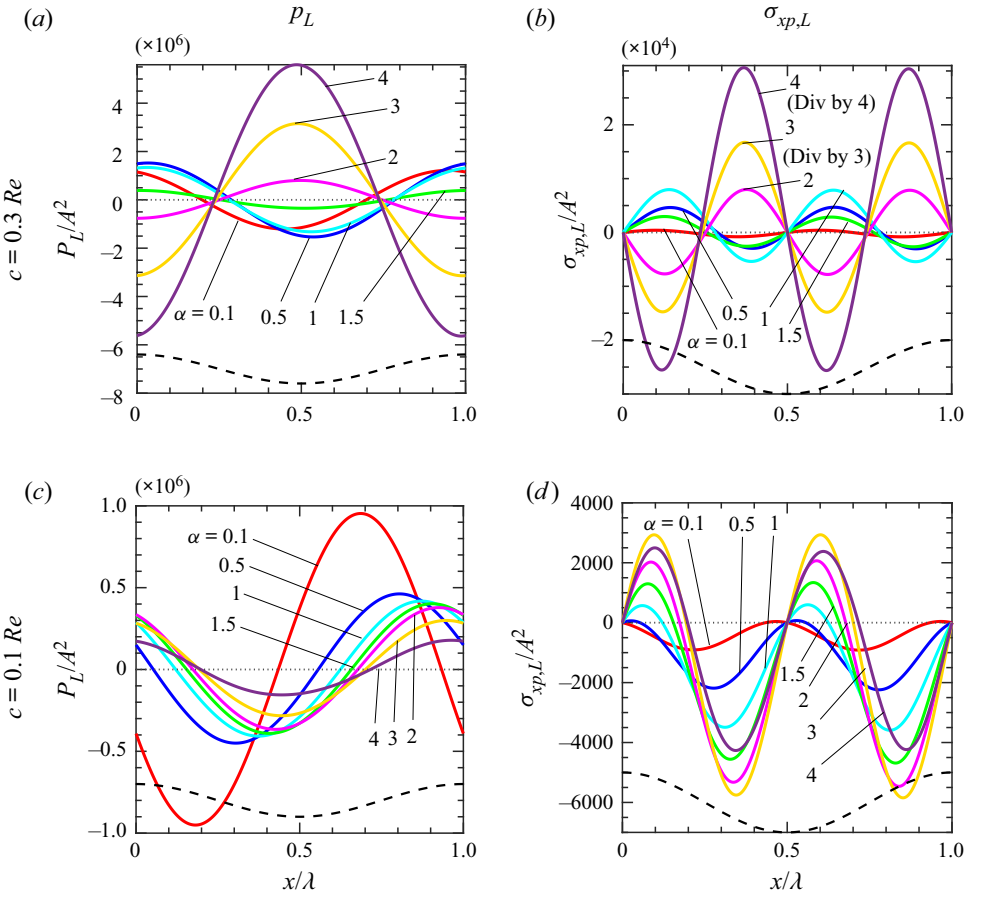

Figure 15. The distributions of the surface pressure at the lower plate p_L (*a*,*c*) and the x component of the pressure force acting on the fluid at the lower plate $\sigma_{xp,L}$ (*b*,*d*). All results are for $Re = 500$ and $A = 0.01$.

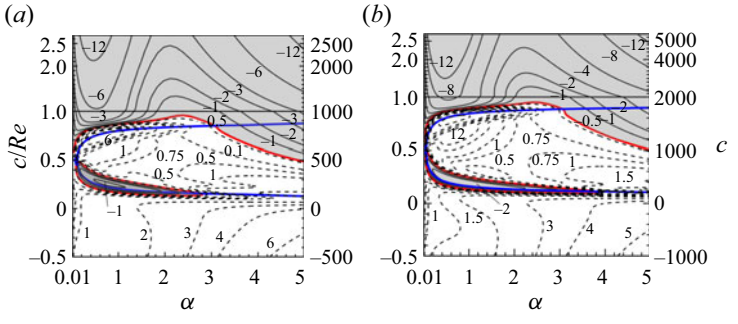

Figure 16. The normalized force correction $F_{norm} = (F_1/ReF_0A^2)$ as a function of α and c for the two Reynolds numbers (*a*) $Re = 1000$ and (*b*) $Re = 2000$. The grey shading identifies resistance-reducing conditions while the red lines show the parameters for which $F_1 = 0$. The regions between the blue lines denote the range of natural frequencies of the Orr–Sommerfeld modes.

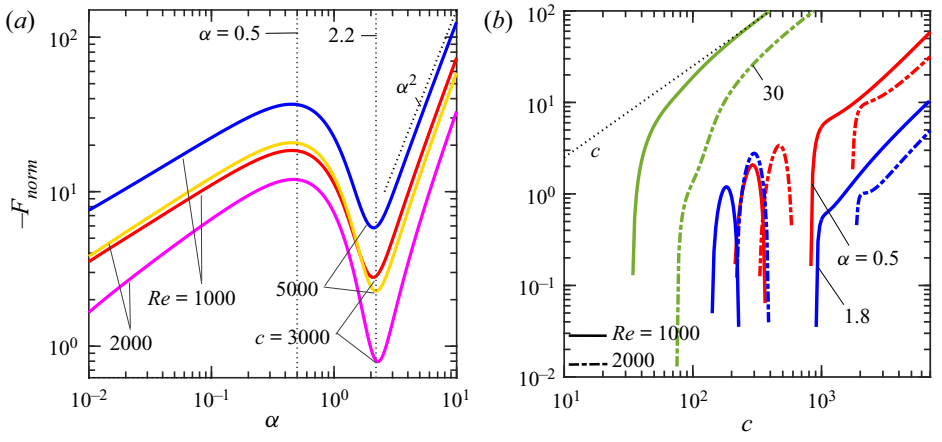

Figure 17. The normalized force correction $F_{norm} = F_1/ReF_0A^2$. (*a*) This quantity plotted as a function of α for the two Reynolds numbers used in figure 16 and the two wave speeds $c = 3000$ and $c = 5000$. (*b*) The normalized force as a function of c for the wavenumbers $\alpha = 0.5$, 1.8 and 30.

We conclude our brief look at the fast-wave problem by examining the various energy terms relevant to the vibrations. The distributions in figure 18 show significant complexity for subcritical waves owing to phase changes between the wave and pressure patterns. These structures are somewhat reminiscent of those relating to flows and are like those when $100 \leq Re < 1000$ so are not discussed further here. There is no net energy saving achieved by these waves.

8. Conclusions

This study has been focused on the question as to whether the use of surface vibrations might constitute a viable alternative propulsion and resistance-reducing method. This has been tackled by attempting to understand the mechanisms that underpin these effects. Our model problem consists of a laminar kinematically driven flow subjected to vibrations at the stationary plate and the key issue is whether the wave changes the external force required to maintain a prescribed upper plate speed. Our chosen vibrations have a very specific structure: they are assumed to be monochromatic waves that are parametrized by a phase speed, an amplitude and the wavenumber. We solved the relevant moving boundary problem using a discretization coupled to the spectrally accurate IBC method used to handle the irregularity of the solution domain. The analytical solution for long waves (see Appendix A) provides some qualitative insight into the flow response.

It has been shown that the upstream-propagating waves always seem to increase the flow resistance but that the situation for downstream-propagating waves is more involved. The calculations show that the waves must be of a certain minimum speed before they can reduce the flow resistance, so it is convenient to distinguish slow and fast waves, with the latter being potentially able to reduce the resistance. While this distinction is adequate at small Reynolds number, as *Re* grows so the picture changes. Increasingly the flow response is affected by the near resonances with the natural flow frequencies; these necessarily correspond to wave speeds less than the upper plate velocity. We can consequently divide the vibration waves into subcritical and supercritical varieties; the resistance reduction achieved by the supercritical waves appears to be proportional to the wave speed c and to the square of the wave wavenumber α. Of significance, we have

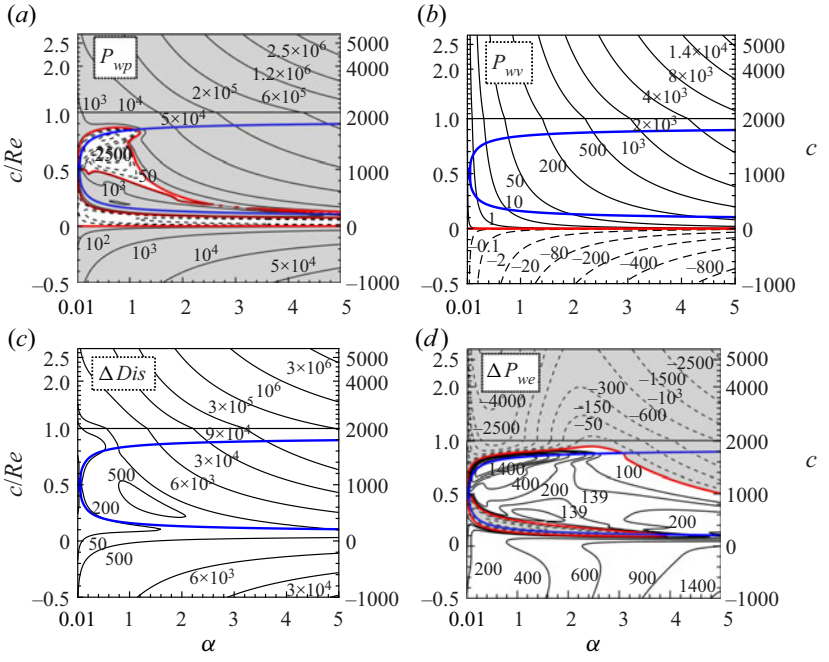

Figure 18. (*a*) The work done by the pressure at the lower plate P_{wp} and (*b*) the work done by viscous forces at the lower plate P_{wv}. (*c*) The increase of dissipation above its reference value and (*d*) the change in power ΔP_{we} required to drive the upper plate. Solid (dashed) lines represent positive (negative) values. The red lines denote zero contours and the zones between the blue lines indicate the range of natural frequencies of the Orr–Sommerfeld modes. All results given are for $Re = 2000$ and $A = 0.01$. The grey shading identifies the region of $P_{wp} > 0$ in (*a*) and $\Delta P_{we} < 0$ in (*d*).

seen that it is theoretically possible to reduce the resistance down to zero if the waves are sufficiently short and fast. While the effect of supercritical waves can be summarized relatively neatly, the corresponding situation for subcritical waves is rather less clear-cut. Most subcritical waves seem to increase the flow resistance albeit the parameter space is punctuated with small pockets within which the flow resistance is mitigated. These effects are characterized by a phase shift between the surface pressure and the wave and have been documented for $Re \leq 2000$. Such waves could be of interest when mixing intensification is desired.

The reduction of resistance can be viewed as a propulsion augmentation strategy in which energy is spent not on the propulsion by itself, but rather on the reduction of resistance which potentially improves system performance. The results show that while the waves reduce resistance, they increase the overall energy expenditure. It seems that the use of fast, short waves is desirable to achieve the maximum resistance reduction. This suggests that one way to advance our knowledge of this process is to develop rational asymptotic theories that might shed light on the various mechanisms at work. While we describe the appropriate long-wavelength structure in Appendix A, there is the potential to conduct short-wavelength ($\alpha \gg 1$) or high-speed ($c \gg 1$) studies of the governing system of equations. Work in these areas has been started and it is hoped that results will help clarify some of the issues that have been uncovered by the largely numerical work described herein. Further computational studies are suggested that might improve the energy efficiency by exploring the effect of changing the properties of the vibration

waves. Here we have looked at simple monochromatic wave shapes, but it is almost certain that improved propulsion augmentation could be achieved with the use of a more carefully chosen mode of vibration.

Acknowledgements. This work has been carried out with support from NSERC. The authors would like to thank Dr A. Bassom from the University of Tasmania for careful review of the text as well as the unnamed reviewers for their suggestions which resulted in a significant improvement of the presentation.

Funding. This work was supported by the Natural Sciences and Engineering Research of Canada (NSERC).

Declaration of interest. The authors report no conflict of interest.

Author ORCIDs.
J.M. Floryan https://orcid.org/0000-0003-3296-4122;
N.N. Haq https://orcid.org/0000-0002-5934-791X.

Appendix A. Long-wavelength vibrations

In this appendix we outline the analytical solution of the flow problem in the case of long-wavelength vibrations. In view of the geometry of the domain, we introduce the new coordinates

$$\eta = (y-1)[1-\tfrac{1}{2}A\cos(\alpha x)]^{-1}+1, \quad \xi = \alpha x, \tag{A1a,b}$$

which map the irregular region into the strip $\eta \in -1, 1$. The field equations then become

$$\frac{\partial^2 u}{\partial \eta^2}+[F_1-F_2(u-c)-F_3 v]\frac{\partial u}{\partial \eta}+F_4\frac{\partial^2 u}{\partial \xi\,\partial \eta}+F_5\frac{\partial^2 u}{\partial \xi^2} -F_6(u-c)\frac{\partial u}{\partial \xi}-F_6\frac{\partial p}{\partial \xi}-F_2\frac{\partial p}{\partial \eta}=0, \tag{A2a}$$

$$\frac{\partial^2 v}{\partial \eta^2}+[F_1-F_2(u-c)-F_3 v]\frac{\partial v}{\partial \eta}+F_4\frac{\partial^2 v}{\partial \xi\,\partial \eta}+F_5\frac{\partial^2 v}{\partial \xi^2}-F_6(u-c)\frac{\partial v}{\partial \xi}-F_3\frac{\partial p}{\partial \eta}=0, \tag{A2b}$$

$$\alpha\frac{\partial u}{\partial \xi}+F_7\frac{\partial u}{\partial \eta}+F_8\frac{\partial v}{\partial \eta}=0, \tag{A2c}$$

in which the coefficients F_1–F_8 are defined by

$$F_1=\eta_{xx}G_3^{-1}=[-\alpha^2 G_1 A\cos(\xi)+2\alpha^2A^2\sin^2(\xi)](\eta-1)G_2^{-1}$$
$$=\tfrac{1}{4}\alpha^2[-G_1A\cos(\xi)+2A^2\sin^2(\xi)](\eta-1)+O(\alpha^4), \tag{A3a}$$

$$F_2=\eta_x G_3^{-1}=-\alpha\, A\sin(\xi)G_1(\eta-1)G_2^{-1}=-\tfrac{1}{4}\alpha\, G_1A\sin(\xi)(\eta-1)+O(\alpha^3), \tag{A3b}$$

$$F_3=\eta_y G_3^{-1}=2\,G_1G_2^{-1}=\tfrac{1}{2}\,G_1-\tfrac{1}{8}\,G_1(G_2-4)+O(\alpha^4), \tag{A3c}$$

$$F_4=2\alpha\eta_x G_3^{-1}=-2\alpha^2 A\sin(\xi)G_1(\eta-1)G_2^{-1}=-\tfrac{1}{2}\alpha^2G_1A\sin(\xi)(\eta-1)+O(\alpha^4), \tag{A3d}$$

$$F_5=\alpha^2G_3^{-1}=\alpha^2G_1^2G_2^{-1}=\tfrac{1}{4}\alpha^2G_1^2+O(\alpha^4), \tag{A3e}$$

$$F_6=\alpha\,G_3^{-1}=\alpha\,G_1^2G_2^{-1}=\tfrac{1}{4}\alpha\,G_1^2+O(\alpha^3), \tag{A3f}$$

$$F_7=\eta_x=-\alpha\,A(\eta-1)\sin(\xi)G_1^{-1}, \quad F_8=\eta_y=2G_1^{-1}, \tag{A3g,h}$$

and in which

$$G_1 \equiv 2 - A\,\cos(\xi), \quad G_2 \equiv 4 + \alpha^2 A^2 \sin^2(\xi)(\eta - 1)^2 \quad \text{and} \quad G_3 \equiv \eta_x^2 + \eta_y^2. \tag{A3i–k}$$

The boundary conditions and the mean pressure constraint then become

$$u(1) = Re, \quad v(1) = 0, \quad u(-1) = 0, \quad v(-1) = c\,A\,\alpha\sin(\xi), \tag{A4a–d}$$

$$\left\{\alpha\frac{\partial p}{\partial \xi} + \frac{A\sin(\xi)}{2 - A\,\cos(\xi)}(1-\eta)\frac{\partial p}{\partial \eta}\right\}_m = 0. \tag{A4e}$$

We expand the unknowns in the forms

$$(u, v) = (\tilde{u}_0, \tilde{v}_0) + \alpha(\tilde{u}_1, \tilde{v}_1) + O(\alpha^2), \quad p = \alpha^{-1}\tilde{p}_{-1} + \tilde{p}_0 + O(\alpha), \tag{A5a,b}$$

$$F = \tilde{F}_0 + \alpha\tilde{F}_1 + 0(\alpha^2), \quad Q_{mean} = \tilde{Q}_{m,0} + \alpha\tilde{Q}_{m,1} + 0(\alpha^2), \tag{A5c,d}$$

where the subscript m is used to denote a mean value. If expansions (A5) are substituted into (A2), we find that

$$\frac{\partial^2\tilde{u}_0}{\partial\eta^2} - \frac{1}{2}\,G_1\tilde{v}_0\frac{\partial\tilde{u}_0}{\partial\eta} - \frac{1}{4}G_1^2\frac{\partial\tilde{p}_{-1}}{\partial\xi} + \frac{1}{4}\,A\,\sin(\xi)\,G_1(\eta-1)\frac{\partial\tilde{p}_{-1}}{\partial\eta} = 0, \tag{A6a}$$

$$\frac{\partial\tilde{p}_{-1}}{\partial\eta} = 0, \quad \frac{\partial\tilde{v}_0}{\partial\eta} = 0, \tag{A6b,c}$$

$$\tilde{v}_0(1) = 0, \quad \tilde{u}_0(1) = Re, \quad \tilde{u}_0(-1) = 0, \quad \tilde{v}_0(-1) = 0,$$

$$\left\{\frac{\partial\tilde{p}_{-1}}{\partial\xi} + \frac{A\sin(\xi)}{2 - A\,\cos(\xi)}(1-\eta)\frac{\partial\tilde{p}_{-1}}{\partial\eta}\right\}_{mean} = 0, \tag{A6d–h}$$

whose solution can be written as

$$\tilde{u}_0 = \frac{1}{8}\,G_1^2\frac{\mathrm{d}\tilde{p}_{-1}}{\mathrm{d}\xi}(\eta^2 - 1) + \frac{1}{2}Re(1+\eta), \quad \tilde{v}_0 = 0, \quad \tilde{p}_{-1} = g_{-1}(\xi), \tag{A7a–c}$$

and in which the form of function $g_{-1}(\xi)$ remains to be fixed. In the light of (A6*b*) the pressure gradient constraint (A6*h*) becomes simply

$$\left.\frac{\mathrm{d}\tilde{p}_{-1}}{\mathrm{d}\xi}\right|_{mean} = 0. \tag{A8}$$

To satisfy this requirement we derive an expression for variations in the function $\tilde{\psi}$ defined by

$$u = \frac{\partial\tilde{\psi}}{\partial y}, \quad v = -\frac{\partial\tilde{\psi}}{\partial x}. \tag{A9a,b}$$

Along the lower plate we have that

$$\mathrm{d}\tilde{\psi} = \frac{\partial\tilde{\psi}}{\partial x}\,\mathrm{d}x + \frac{\partial\tilde{\psi}}{\partial y}\,\mathrm{d}y = -v\,\mathrm{d}x = c\frac{\mathrm{d}y_L}{\mathrm{d}x} = -\alpha cA\sin(\xi), \tag{A10}$$

so that one integration gives

$$\tilde{\psi}_L = cA\cos(\xi) + C_L, \tag{A11}$$

where C_L is an integration constant and which is the mean value of $\tilde{\psi}_L$ along the plate. Furthermore, we know that $\tilde{\psi}$ is constant along the upper plate so that

$$\tilde{\psi}_U = C_U, \tag{A12}$$

where C_U is a second unknown constant. One of these constants can be chosen arbitrarily while the other needs to be determined using the zero mean pressure gradient constraint.

If we subtract (A11) from (A12) we have

$$\tilde{\psi}_U - \tilde{\psi}_L = C_U - C_L - cA\cos(\xi) = \tilde{Q}_{m,0} - cA\cos(\xi). \tag{A13}$$

This difference may alternatively be found using the expression for the flow rate that follows from integrating the x velocity across the slot. Then

$$\tilde{\psi}_U - \tilde{\psi}_L = \int_{y_L}^{y_U} \tilde{u}_0 \,\mathrm{d}y = \frac{1}{2}\int_{-1}^{1} [2 - A\cos(\xi)]\tilde{u}_0 \,\mathrm{d}\eta = -\frac{1}{12}[2 - A\cos(\xi)]^3 \frac{\mathrm{d}\tilde{p}_{-1}}{\mathrm{d}\xi} + \frac{1}{2}[2 - A\cos(\xi)]Re, \tag{A14}$$

and results (A13) and (A14) together show that

$$\frac{\mathrm{d}\tilde{p}_{-1}}{\mathrm{d}\xi} = -\frac{12\tilde{Q}_{m,0}}{[2 - A\cos(\xi)]^3} + \frac{12c\,A\cos(\xi)}{[2 - A\cos(\xi)]^3} + \frac{6Re}{[2 - A\cos(\xi)]^2}. \tag{A15}$$

The mean value of this pressure gradient is

$$\left.\frac{\mathrm{d}\tilde{p}_{-1}}{\mathrm{d}\xi}\right|_{mean} = -\frac{6\tilde{Q}_{m,0}(8 + A^2)}{(4 - A^2)^{5/2}} + \frac{36cA^2}{(4 - A^2)^{5/2}} + \frac{12Re}{(4 - A^2)^{3/2}}, \tag{A16}$$

and for this to equal zero requires that

$$\tilde{Q}_{m,0} = c\frac{6\,A^2}{8 + A^2} + Re\frac{2(4 - A^2)}{8 + A^2}. \tag{A17}$$

The substitution of expression (A17) into (A7) leads to the determination of $\tilde{u}_0$ and the other quantities of interest so that

$$\tilde{u}_0 = \frac{3}{4}Re\left[1 - \frac{4(4 - A^2)}{(8 + A^2)[2 - A\cos(\xi)]}\right](\eta^2 - 1) + c\frac{A}{2 - A\cos(\xi)}\left[\frac{3}{2}\cos(\xi) - \frac{9A}{8 + A^2}\right](\eta^2 - 1) + \frac{1}{2}Re(\eta + 1), \tag{A18}$$

while the pressure term is

$$\tilde{p}_{-1} = Re\frac{6A\sin(\xi)}{(4 - A^2)[2 - A\cos(\xi)]^2}\left[\frac{-32 + 2A^2 + 12A\cos(\xi)}{8 + A^2} + 2 - A\ \cos(\xi)\right] + c\frac{12A\sin(\xi)}{(4 - A^2)^2[2 - A\cos(\xi)]^2} \times \left[\frac{3A^2}{8 + A^2}[-16 + A^2 + 6A\cos(\xi)] + 8 + A^2 - A(2 + A^2)\ \cos(\xi)\right]. \tag{A19}$$

We can then determine the viscous and pressure parts of the stress at the lower and upper plates to be

$$\sigma_{xv,L} = \tilde{\sigma}_{xv0,L} + 0(\alpha) = Re\frac{2}{2 - A\ \cos(\xi)}\left[1 - \frac{6(4 - A^2)}{(8 + A^2)[2 - A\ \cos(\xi)]}\right] + c\frac{6A}{[2 - A\ \cos(\xi)]^2}\left[\cos(\xi) - \frac{6A}{8 + A^2}\right] + 0(\alpha), \tag{A20a}$$

$$\sigma_{xv,U} = \tilde{\sigma}_{xv0,U} + 0(\alpha) = Re\frac{4}{2 - A\cos(\xi)}\left[1 - \frac{3(4 - A^2)}{(8 + A^2)[2 - A\cos(\xi)]}\right] + c\frac{6A}{[2 - A\cos(\xi)]^2}\left[\cos(\xi) - \frac{6A}{8 + A^2}\right] + 0(\alpha)\ , \tag{A20b}$$

$$\sigma_{xp,L} = \tilde{\sigma}_{xp0,L} + 0(\alpha) = Re\frac{6A^2\sin^2(\xi)}{(4 - A^2)[2 - A\cos(\xi)]^2} \times \left[\frac{-32 + 2A^2 + 12A\cos(\xi)}{8 + A^2} + 2 - A\ \cos(\xi)\right] + c\frac{12A^2\sin^2(\xi)}{(4 - A^2)^2[2 - A\ \cos(\xi)]^2} \times \left[\frac{3A^2}{8 + A^2}[-16 + A^2 + 6A\cos(\xi)] + 8 + A^2 - A(2 + A^2)\cos(\xi)\right] + 0(\alpha), \tag{A20c}$$

and the total forces (per unit width and unit length) are given by

$$F_{xv,L} = \tilde{F}_{xv0,L} + 0(\alpha) = -\frac{2Re(4 - A^2) + 6cA^2}{(8 + A^2)(4 - A^2)^{1/2}} + 0(\alpha),$$

$$F_{xp,L} = \tilde{F}_{xp0,L} + 0(\alpha) = \frac{-6ReA^2 + 12cA^2}{(8 + A^2)(4 - A^2)^{1/2}} + 0(\alpha), \tag{A21a,b}$$

$$F = \tilde{F}_0 + 0(\alpha) = \frac{4Re(2 + A^2) - 6cA^2}{(8 + A^2)(4 - A^2)^{1/2}} + 0(\alpha). \tag{A21c}$$

The next-order system can be cast as

$$\frac{\partial^2\tilde{u}_1}{\partial\eta^2} - \frac{1}{2}G_1\frac{\partial\tilde{u}_o}{\partial\eta}\tilde{v}_1 - \frac{1}{4}G_1^2\frac{\partial\tilde{p}_0}{\partial\xi} + \frac{1}{4}A\ \sin(\xi)G_1(\eta - 1)\frac{\partial\tilde{p}_0}{\partial\eta} = -\frac{1}{4}\ A\ \sin(\xi)G_1(\eta - 1)(\tilde{u}_0 - c)\frac{\partial\tilde{u}_0}{\partial\eta} + \frac{1}{4}\ G_1^2(\tilde{u}_0 - c)\frac{\partial\tilde{u}_0}{\partial\xi}, \tag{A22a}$$

$$\frac{\partial\tilde{v}_1}{\partial\eta} = \frac{1}{2}A(\eta - 1)\sin(\xi)\frac{\partial\tilde{u}_0}{\partial\eta} - \frac{1}{2}G_1\frac{\partial\tilde{u}_0}{\partial\xi}, \quad \frac{\partial\tilde{p}_0}{\partial\eta} = 0, \tag{A22b,c}$$

$$\eta = 1:\ \tilde{u}_1 = 0, \quad \tilde{v}_1 = 0, \tag{A22d,e}$$

$$\eta = -1:\ \tilde{u}_1 = 0, \quad \tilde{v}_1 = c\ A\ \sin(\xi), \tag{A22f,g}$$

$$\left\{\frac{\partial\tilde{p}_0}{\partial\xi} + \frac{A\sin(\xi)}{2 - A\cos(\xi)}(1 - \eta)\frac{\partial\tilde{p}_0}{\partial\eta}\right\}_{mean} = 0. \tag{A22h}$$

We remark that this system does not contribute to mean quantities as it admits only purely periodic solutions.

The primary quantity of interest is the force F which needs to be applied to the upper plate to maintain its movement. The component of this force that can be attributed to the vibrations is

$$F_1 = \tilde{F}_0 - \frac{1}{2}Re + 0(\alpha^2) = Re\left[\frac{4(2+A^2)}{(8+A^2)(4-A^2)^{1/2}} - \frac{1}{2}\right] - c\frac{6A^2}{(8+A^2)(4-A^2)^{1/2}} + 0(\alpha^2), \tag{A23}$$

while the part of the flow rate owing to vibrations is

$$Q_{1,mean} = \tilde{Q}_{m,0} - Re + 0(\alpha^2) = c\frac{6\,A^2}{8+A^2} - Re\frac{3A^2}{8+A^2} + 0(\alpha^2). \tag{A24}$$

The flow topology possesses numerous interesting features exemplified within the result

$$\begin{aligned}\psi = {} & \frac{3}{8}Re\left[2 - A\cos(\xi) - \frac{4(4+A^2)}{8+A^2}\right]\left(\frac{1}{3}\eta^3 - \eta + \frac{2}{3}\right) \\ & + \frac{1}{4}Re[2 - A\cos(\xi)]\left(\frac{1}{2}\eta^2 + \eta - \frac{3}{2}\right) \\ & + \frac{1}{2}cA\left[\frac{3}{2}\cos(\xi) - \frac{3A}{8+A^2}\right]\left(\frac{1}{3}\eta^3 - \eta + \frac{2}{3}\right) - \frac{1}{2}c[2 - A\cos(\xi)](\eta - 1),\end{aligned} \tag{A25}$$

which can be viewed as the stream function expressed within the moving reference frame. The conditions that lead to the formation of separation zones near the vibrating plate can be found by looking for a zero in the normal-to-plate velocity derivative. The relevant expression is precisely that for the shear stress $\sigma_{t,L}$ acting on this plate:

$$\sigma_{t,L} = \boldsymbol{\sigma}_L \cdot \boldsymbol{t}_L = [\sigma_{x,L}, \sigma_{y,L}][t_{x,L}, t_{y,L}]^T = \frac{2Re}{2 - A\cos(\xi)}\left[1 - \frac{6(4-A^2)}{(8+A^2)[2 - A\cos(\xi)]}\right] + \frac{4Ac}{[2 - A\ \cos(\xi)]^2}\left[\frac{3}{2}\cos(\xi) - \frac{9A}{8+A^2}\right]; \tag{A26}$$

here $\boldsymbol{t}_L$ is the unit vector tangential to the plate with components $t_{x,L} = N_L$, $t_{y,L} = N_L(\mathrm{d}f/\mathrm{d}x)$ and the subscript T denotes the usual transpose. If we demand that $\sigma_{t,L} = 0$ we have

$$\cos(\xi) = \frac{8Re(1-A^2) + 18cA^2}{A(8+A^2)(3c - Re)}, \tag{A27}$$

and the requirement $|\cos\xi| \leq 1$ tells us if and where separation may take place for a given combination of flow parameters (Re, A, c). For stationary waves $c = 0$ separation occurs whenever $A > -3 + \sqrt{13} \approx 0.606$ and $\xi = \pi$ is the incipient point irrespective of the value of Re (Floryan et al. 2021). To identify separation points in a more general setting, it

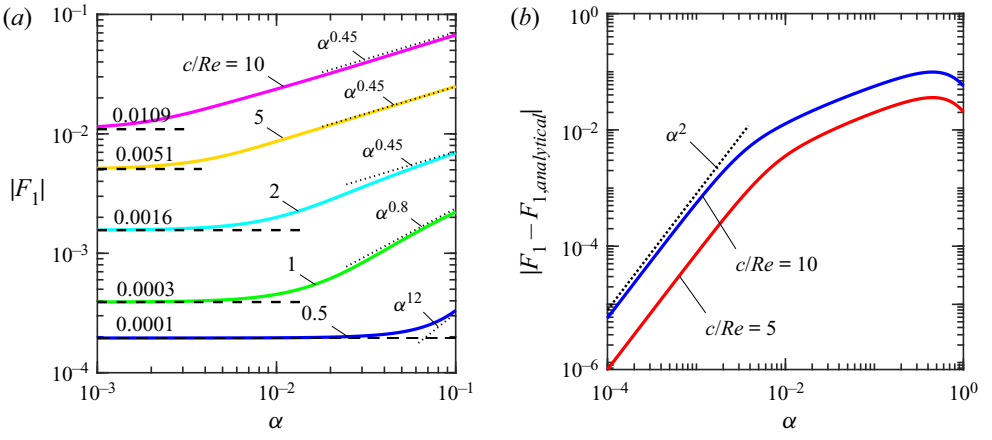

Figure 19. (*a*) The magnitude of the force correction $|F_1|$ and (*b*) the difference between the numerically and analytically ($F_{1,analytical}$) determined force corrections $|F_1 - F_{1,analytical}|$. Results shown as functions of α for the parameter choices $Re = 500$, $A = 0.0025$ and the five values $c/Re = 0.5$, 1, 2, 5 and 10. There is evidence of the emergence of a zone in which $|F_1|$ varies proportional to $\alpha^{0.45}$ for the larger values of c prior to the analytical small-α limit is reached.

is helpful to recast (A18) as

$$\tilde{u}_0/Re = \frac{3}{4}\left[1 - \frac{4(4-A^2)}{(8+A^2)[2-A\ \cos(\xi)]}\right](\eta^2-1) + \hat{c}\frac{A}{2-A\ \cos(\xi)}\left[\frac{3}{2}\cos(\xi) - \frac{9A}{8+A^2}\right](\eta^2-1) + \frac{1}{2}(\eta+1), \tag{A28}$$

where $\hat{c} = c/Re$. It is evident that $\tilde{u}_0$ is an even function of ξ and it is therefore sufficient to consider $\xi = 0$ (a wave crest) and $\xi = \pi$ (a wave trough) to identify the onset conditions. Routine analysis shows that separation at the crest can be produced only by waves with phase speed $c/Re > (A^2 - 6A - 4)/3A(A-4)$ and these waves propagate in the same direction as the upper plate. The situation at the trough is more complex as waves that propagate forward can induce separation only if they are not too fast, $c/Re < (A^2 + 6A - 4)/3A(A+4)$, and only then if they are of sufficient amplitude $A > -3 + \sqrt{13}$. Waves that propagate backwards can lead to separation if their phase velocity is sufficiently negative $c/Re < (A^2 + 6A - 4)/3A(A+4)$, and their amplitude is not too large $A < -3 + \sqrt{13}$. These results prove that it is not possible to have a reflux situation in which there is a stream tube that carries fluid in the direction opposite to the movement of the upper plate.

In passing we mention that waves which propagate both forward and backward can theoretically capture fluid in boluses and transport it at the speed of the wave if the amplitude of the wave is large. Proof of the existence of boluses relies on numerical work but this is not pursued here as the focus of our analysis is on waves at amplitudes well below the typical bolus-formation threshold.

A comparison of the numerical and analytic solutions is presented in figure 19 and provides a benchmark for assessing the likely range over which the small-α solution is reasonably accurate This range seems to decrease as the ratio c/Re grows and tests confirm that our analytic solution is correct to $O(\alpha)$ with error of size $O(\alpha^2)$.

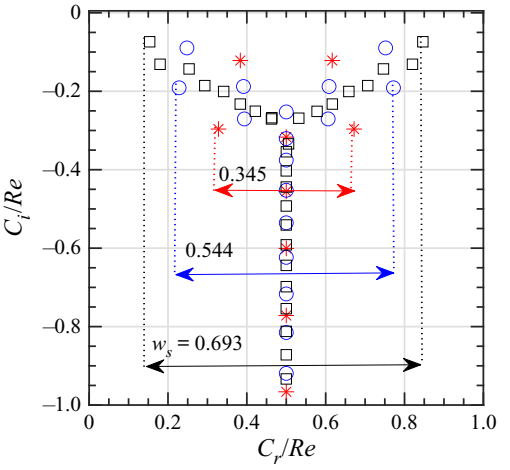

Figure 20. Spectra of the Orr–Sommerfeld problem when $Re = 500$ and the three wavenumbers $\alpha = 0.5$ (red stars), 1.7 (blue circles) and 5 (black squares). The horizontal arrows show the distance w_s between the fastest and the slowest wave for a given α.

Appendix B. The natural frequencies of Couette flow

In this appendix we sketch the method used to determine the natural flow frequencies of the underlying Couette flow. Consider small unsteady disturbances that are superposed on the flow between two parallel smooth plates with the upper plate moving with a prescribed velocity while the lower plate is stationary. The flow quantities can be written as

$$\left.\begin{gathered}\boldsymbol{v}(X,Y,t) = [u(X,Y,t), v(X,Y,t)] = [\tfrac{1}{2}Re(1+Y) + u_1(X,Y,t), v_1(X,Y,t)], \\ p(X,Y,t) = p_0 + p_1(X,Y,t).\end{gathered}\right\} \tag{B1a,b}$$

The substitution of expressions (B1) in (2.2), followed by linearization and the assumption of the wave form ansatz

$$[u_1, v_1, p_1](X,Y,t) = [\hat{u}_1, \hat{v}_1, \hat{p}_1](Y)\,\mathrm{e}^{\mathrm{i}\alpha(X-Ct)} + \text{complex conjugate}, \tag{B2}$$

leads to the standard Orr–Sommerfeld problem:

$$\begin{gathered}[(D^2-\alpha^2)^2 - \tfrac{1}{2}\mathrm{i}\alpha(Re(1+Y) - 2C)(D^2-\alpha^2)]\hat{v}_1 = 0 \quad \text{subject to } \hat{v}_1(\pm 1) = 0, \\ D\hat{v}_1(\pm 1) = 0.\end{gathered} \tag{B3}$$

Here $D \equiv \mathrm{d}/\mathrm{d}Y$ and the wave phase speed C_r, which is the real part of C, is bounded according to Howard's semicircle theorem so that $0 < C_r < Re$ (Schmid & Henningson 2001).

The solutions of the eigenproblem (B3) describe the possible Tollmien–Schlichting waves. It was solved numerically by writing the unknowns as Chebyshev expansions and then constructing linear algebraic equations for the expansion coefficients using the Galerkin projection method. Boundary conditions were enforced using the τ-procedure (Canuto et al. 1992) and the spectral decomposition of the coefficient matrix was achieved using standard methods (Garbow et al. 1977; Moler 2004). The inverse iteration technique was used to enhance the accuracy of the computed eigenvalues when necessary (Moradi & Floryan 2014). It is known that these disturbances are attenuated (Romanov 1972) so their long-term existence requires a continuous energy input.

Some typical spectra of the Orr–Sommerfeld problem are depicted in figure 20. The distance w_s between the fastest and the slowest disturbances is marked in some figures in the main text (see, for example, figure 6*b*).

References

Abtahi, A. & Floryan, J.M. 2017 Natural convection and thermal drift. *J. Fluid Mech.* **826**, 553–582.

Ali, N., Ullah, K. & Rasool, H. 2020 Bifurcation analysis for a two-dimensional peristaltic driven flow of power-law fluid in asymmetric channel. *Phys. Fluids* **32**, 073104.

Asai, M. & Floryan, J.M. 2006 Experiments on the linear instability of flow in a wavy channel. *Eur. J. Mech.* (B/*Fluids*) **25**, 971–986.

Bewley, T.R. 2009 A fundamental limit on the balance of power in a transpiration-controlled channel flow. *J. Fluid Mech.* **632**, 443–446.

Blake, J.R. & Sleigh, M.A. 1974 Mechanics of ciliary locomotion. *Biol. Rev.* **49**, 85–125.

Brennen, C. & Winet, H. 1977 Fluid mechanics of propulsion by cilia and flagella. *Annu. Rev. Fluid Mech.* **9**, 339–398.

Cabal, A., Szumbarski, J. & Floryan, J.M. 2001 Numerical simulation of flows over corrugated walls. *Comput. Fluids* **30**, 753–776.

Canuto, C., Hussaini, M.Y., Quarteroni, A. & Zang, T.A. 1992 *Spectral Methods in Fluid Dynamics*. Springer.

Cattafesta, L.N. & Sheplak, M. 2011 Actuators for active flow control. *Annu. Rev. Fluid Mech.* **43**, 247–272.

Chan, B., Balmforth, N.J. & Hosoi, A.E. 2005 Lubrication and adhesive locomotion. *Phys. Fluids* **19**, 113101.

Chen, Y., Floryan, J.M., Chew, Y.T. & Khoo, B.C. 2016 Groove-induced changes of discharge in channel flows. *J. Fluid Mech.* **799**, 297–333.

DeGroot, C.T., Wang, C. & Floryan, J.M. 2016 Drag reduction due to streamwise grooves in turbulent channel flow. *Trans. ASME J. Fluid Engng* **138**, 121201.

Deguchi, K. & Nagata, M. 2011 Bifurcations and instabilities in sliding Couette flow. *J. Fluid Mech.* **678**, 156–178.

Floryan, J.M. 2002 Centrifugal instability of Couette flow over a wavy wall. *Phys. Fluids* **14**, 312–322.

Floryan, J.M. 2003 Wall-Transpiration-induced instabilities in plane Couette flow. *J. Fluid Mech.* **488**, 151–188.

Floryan, J.M. 2007 Three-dimensional instabilities of laminar flow in a rough channel and the concept of hydraulically smooth wall. *Eur. J. Mech.* (B/*Fluids*) **26**, 305–329.

Floryan, J.M., Faisal, M. & Panday, S. 2021 On the peristaltic pumping. *Phys. Fluids* **33**, 033609.

Floryan, D. & Floryan, J.M. 2015 Drag reduction in heated channels. *J. Fluid Mech.* **765**, 353–395.

Floryan, J.M. & Inasawa, A. 2021 Pattern interaction effect. *Sci. Rep.* **11**, 14573.

Floryan, J.M. & Rasmussen, H. 1989 Numerical analysis of viscous flows with free surfaces. *Appl. Mech. Rev.* **42**, 323–341.

Floryan, J.M., Shadman, S. & Hossain, M.Z. 2018 Heating-induced drag reduction in relative movement of parallel plates. *Phys. Rev. Fluids* **3**, 094101.

Floryan, J.M., Szumbarski, J. & Wu, X. 2002 Stability of flow in a channel with vibrating walls. *Phys. Fluids* **14**, 3927–3936.

Floryan, J.M. & Zandi, S. 2019 Reduction of pressure losses and increase of mixing in laminar flows through channels with long-wavelength vibrations. *J. Fluid Mech.* **864**, 670–707.

Fukagata, K., Sugiyama, K. & Kasagi, N. 2009 On the lower bound of net driving power in controlled duct flows. *Physica* D **338**, 1082–1086.

Fukunishi, Y. & Ebina, I. 2001 Active control of boundary-layer transition using a thin actuator. *JSME Intl J.* **44**, 24–29.

Fung, Y.C. & Yih, C.S. 1968 Peristaltic transport. *J. Appl. Mech.* **35**, 669–675.

Garbow, B.S., Boyle, J.M., Dongarra, J.J. & Moler, C.B. 1977 *Matrix Eigensystem Routines – EISPACK Guide Extension*. Lecture Notes in Physics, vol. 51. Springer-Verlag.

Gepner, S.W. & Floryan, J.M. 2020 Use of surface corrugations for energy-efficient chaotic stirring in low Reynolds number flows. *Sci. Rep.* **10**, 8965.

Gittler, P. 1993 Stability of Poiseuille–Couette flow between concentric cylinders. *Acta Mech.* **101**, 1–13.

Gropper, D., Wang, L. & Harvey, T.J. 2016 Hydrodynamic lubrication of textured surfaces: a review of modeling techniques and key findings. *Tribol. Intl* **94**, 509–529.

HOEPFFNER, J. & FUKAGATA, K. 2009 Pumping or drag reduction. *J. Fluid Mech.* **635**, 171–187.
HOSSAIN, M.Z., FLORYAN, D. & FLORYAN, J.M. 2012 Drag reduction due to spatial thermal modulations. *J. Fluid Mech.* **713**, 398–419.
HUSAIN, S.Z. & FLORYAN, J.M. 2008*a* Gridless spectral algorithm for Stokes flow with moving boundaries. *Comput. Meth. Appl. Mech. Engng* **198**, 245–259.
HUSAIN, S.Z. & FLORYAN, J.M. 2008*b* Implicit spectrally accurate method for moving boundary problems using immersed boundary conditions concept. *J. Comput. Phys.* **227**, 4459–4477.
HUSAIN, S.Z. & FLORYAN, J.M. 2010 Spectrally-accurate algorithm for moving boundary problems for the Navier-Stokes equations. *J. Comput. Phys.* **229**, 2287–2313.
HUSAIN, S.Z., SZUMBARSKI, J. & FLORYAN, J.M. 2009 Over-constrained formulation of the immersed boundary condition method. *Comput. Meth. Appl. Mech. Engng* **199**, 94–112.
INASAWA, A., HARA, K. & FLORYAN, J.M. 2021 Experiments on thermal drift. *Phys. Fluids* **33**, 087116.
INASAWA, A., NINOMIYA, C. & ASAI, M. 2013 Suppression of tonal trailing-edge noise from an airfoil using a plasma actuator. *AIAA J.* **51**, 1695–1702.
JAFFRIN, M.Y. & SHAPIRO, A.H. 1971 Peristaltic pumping. *Annu. Rev. Fluid Mech.* **3**, 13–37.
JIAO, L. & FLORYAN, J.M. 2021 On the use of transpiration for reduction of resistance to relative movement of parallel plates. *Phys. Rev. Fluids* **6**, 014101.
KAITHAKKAL, A.J., KAMETANI, Y. & HASEGAWA, Y. 2020 Dissimilarity between turbulent heat and momentum transfer induced by a streamwise travelling wave of wall blowing and suction. *J. Fluid Mech.* **886**, A29.
KATO, T., FUKUNISHI, Y. & KOBAYASHI, R. 1997 Artificial control of the three-dimensionalization process of T-S waves in boundary-layer transition. *JSME Intl J.* **40**, 536–541.
KATZ, D.F. 1974 On the propulsion of micro-organisms near solid boundaries. *J. Fluid Mech.* **64**, 33–49.
LAUGA, E. 2007 Propulsion in a viscoelastic fluid. *Phys. Fluids* **19**, 083104.
LAUGA, E. 2016 Bacterial hydrodynamics. *Annu. Rev. Fluid Mech.* **48**, 105–135.
LEE, S., BUSH, J.W.M., HOSOI, A.E. & LAUGA, E. 2008 Crawling beneath the free surface: water snail locomotion. *Phys. Fluids* **20**, 082106.
LIEU, B.K., MOARREF, R. & JOVANOVIĆ, M.R. 2010 Controlling the onset of turbulence by streamwise travelling waves. Part 2. Direct numerical simulation. *J. Fluid Mech.* **663**, 100–119.
MAMORI, H., IWAMOTO, K. & MURATA, A. 2014 Effect of parameters of traveling waves created by blowing and suction on the relaminarization phenomena in fully developed turbulent channel flow. *Phys. Fluids* **26**, 015101.
MOARREF, R. & JOVANOVIĆ, M.R. 2010 Controlling the onset of turbulence by streamwise travelling waves. Part 1. Receptivity analysis. *J. Fluid Mech.* **663**, 70–99.
MOHAMMADI, A. & FLORYAN, J.M. 2013*a* Pressure losses in grooved channels. *J. Fluid Mech.* **725**, 23–54.
MOHAMMADI, A. & FLORYAN, J.M. 2013*b* Groove optimization for drag reduction. *Phys. Fluids* **25**, 113601.
MOHAMMADI, A. & FLORYAN, J.M. 2014 Effects of longitudinal grooves on the Couette-Poiseuille flow. *J. Theor. Comput. Fluid Mech.* **28**, 549–572.
MOHAMMADI, A. & FLORYAN, J.M. 2015 Numerical analysis of laminar-drag-reducing grooves. *Trans ASME J. Fluids Engng* **137**, 041201.
MOLER, C.B. 2004 *Numerical Computing with MATLAB*. SIAM.
MORADI, H.V. & FLORYAN, J.M. 2013 Flows in annuli with longitudinal grooves. *J. Fluid Mech.* **716**, 280–315.
MORADI, H.V. & FLORYAN, J.M. 2014 Stability of flow in a channel with longitudinal grooves. *J. Fluid Mech.* **757**, 613–648.
MORADI, H.V. & FLORYAN, J.M. 2016 Sliding Couette flow in a ribbed annulus. *Phys. Fluids* **28**, 074103.
NABAE, Y. & FUKUGATA, K. 2021 Bayesian optimization of traveling wave-like wall deformation for friction drag reduction in turbulent channel flow. *J. Fluid Sci. Tech.* **16**, 21-00307.
NAKANISHI, R., MAMORI, H. & FUKAGATA, K. 2012 Relaminarization of turbulent channel flow using traveling wave-like wall deformation. *Intl J. Heat Fluid Flow* **21**, 152–159.
PEROT, J.B. & ROTHSTEIN, J.P. 2004 Laminar drag reduction in microchannels using ultrahydrophobic surfaces. *Phys. Fluids* **16**, 4635–4643.
ROMANOV, V.A. 1972 Stability of plane-parallel Couette flow. *Funct. Anal. Applics.* **7**, 137–146.
SCHMID, P.S. & HENNINGSON, D.S. 2001 *Stability and Transition in Shear Flows*. Applied Mathematical Sciences, vol. 142. Springer.
SHAPIRO, S., JAFFRIN, M. & WEINBERG, S. 1969 Peristaltic pumping with long wavelengths at low Reynolds numbers. *J. Fluid Mech.* **37**, 799–825.
SZUMBARSKI, J. & FLORYAN, J.M. 1999 A direct spectral method for determination of flows over corrugated boundaries. *J. Comput. Phys.* **153**, 378–402.

TAYLOR, G. 1951 Analysis of the swimming of microscopic organisms. *Proc. R. Soc. Lond.* A **209**, 447–461.
TILLMARK, N. & ALFREDSSON, P. 1992 Experiments on transition in plane Couette flow. *J. Fluid Mech.* **235**, 89–102.
WALSH, M.J. 1983 Riblets as a viscous drag reduction technique. *AIAA J.* **21**, 485–486.
YADAV, N., GEPNER, S.W. & SZUMBARSKI, J. 2021 Determination of groove shape with strong destabilization and low hydraulic drag. *Intl J. Heat Fluid Flow* **87**, 108751.